BTN3A3 evasion promotes the zoonotic potential of influenza A viruses

Article

BTN3A3 evasion promotes the zoonotic potential of influenza A viruses

https://doi.org/10.1038/s41586-023-06261-8

Received: 17 February 2023

Accepted: 25 May 2023

Check for updates

Rute Maria Pinto[1,6], Siddharth Bakshi[1,8], Spyros Lytras[1,8], Mohammad Khalid Zakaria[1,8], Simon Swingler[1], Julie C. Worrell[2], Vanessa Herder[1], Kerrie E. Hargrave[2], Margus Varjak[1,7], Natalia Cameron-Ruiz[1], Mila Collados Rodriguez[1], Mariana Varela[1], Arthur Wickenhagen[1], Colin Loney[1], Yanlong Pei[3], Joseph Hughes[1], Elise Valette[1], Matthew L. Turnbull[1], Wilhelm Furnon[1], Quan Gu[1], Lauren Orr[1], Aislynn Taggart[1], Ola Diebold[4], Chris Davis[1], Chris Boutell[1], Finn Grey[4], Edward Hutchinson[1], Paul Digard[4], Isabella Monne[5], Sarah K. Wootton[3], Megan K. L. MacLeod[2], Sam J. Wilson[1,9] & Massimo Palmarini[1,9]✉

Spillover events of avian influenza A viruses (IAVs) to humans could represent the first step in a future pandemic[1]. Several factors that limit the transmission and replication of avian IAVs in mammals have been identified. There are several gaps in our understanding to predict which virus lineages are more likely to cross the species barrier and cause disease in humans[1]. Here, we identified human BTN3A3 (butyrophilin subfamily 3 member A3)[2] as a potent inhibitor of avian IAVs but not human IAVs. We determined that BTN3A3 is expressed in human airways and its antiviral activity evolved in primates. We show that BTN3A3 restriction acts primarily at the early stages of the virus life cycle by inhibiting avian IAV RNA replication. We identified residue 313 in the viral nucleoprotein (NP) as the genetic determinant of BTN3A3 sensitivity (313F or, rarely, 313L in avian viruses) or evasion (313Y or 313V in human viruses). However, avian IAV serotypes, such as H7 and H9, that spilled over into humans also evade BTN3A3 restriction. In these cases, BTN3A3 evasion is due to substitutions (N, H or Q) in NP residue 52 that is adjacent to residue 313 in the NP structure[3]. Thus, sensitivity or resistance to BTN3A3 is another factor to consider in the risk assessment of the zoonotic potential of avian influenza viruses.

Influenza A viruses (IAVs) cause a substantial global health burden and circulate both in humans and animal species, including domestic poultry, pigs, dogs and horses. Wild aquatic birds are the main natural reservoir of IAVs[4]. Ducks, shorebirds, gulls and other waterbirds harbour 16 haemagglutinin and 9 neuraminidase subtypes[5]. IAVs from wild bird reservoirs can infect economically important birds, such as chickens, turkeys, quail and other gallinaceous species and domestic waterfowl[4]. The population density of domestic birds and the direct exposure to infected birds facilitates avian IAV spillovers into susceptible mammals, including humans. Avian IAVs can also further reassort (that is, exchange genome segments) with viruses established in susceptible species resulting in the rich IAV genetic diversity. In humans, the influenza pandemics of 1918, 1957, 1968 and 2009 were all caused by viruses containing genomic segments of avian origin[6].

Occasionally, spillover of avian IAVs into humans may result in severe or even lethal disease[7]. For example, in 2013 an H7N9 variant resulting from many reassortment events of different avian viruses[8] caused more than 600 human deaths[9] and has since re-emerged in different epidemic waves[10]. These spillover events are not typically followed by extensive human-to-human transmission chains, but they are a risk to global health as they could enable the first step towards human adaptation and the generation of pandemic IAV strains[1].

Several barriers have been identified that hamper avian IAV transmission and adaptation in humans[11]. These include virus haemagglutinin receptor binding specificity[12], higher haemagglutinin pH fusion[13,14], increased efficiency of the virus polymerase in human cells[15], length of the neuraminidase stalk[16,17] and sensitivity to the host antiviral factor Mx1/MxA[11,18,19].

Despite the progress made in the past two decades, gaps remain in understanding what allows certain avian IAV subtypes or lineages to spillover in humans. In this study, we aimed to identify (1) host genetic barriers to avian IAV replication in human cells and (2) IAV genetic signatures that can be directly correlated with their zoonotic potential.

BTN3A3 specifically restricts avian IAVs

We focused on the host type I interferon (IFN) response as it is one of the key host antiviral innate immune mechanisms and a barrier for virus cross-species transmission[20]. IFN acts through the activation of hundreds of IFN stimulated genes (ISGs), some of which have

[1]MRC–University of Glasgow Centre for Virus Research, Glasgow, UK. [2]School of Infection and Immunity, University of Glasgow, Glasgow, UK. [3]Department of Pathobiology, University of Guelph, Guelph, Ontario, Canada. [4]The Roslin Institute, University of Edinburgh, Edinburgh, UK. [5]Istituto Zooprofilattico Sperimentale delle Venezie (IZSVe), Legnaro, Italy. [6]Present address: The Roslin Institute, University of Edinburgh, Edinburgh, UK. [7]Present address: Faculty of Science and Technology, Institute of Technology, University of Tartu, Tartu, Estonia. [8]These authors contributed equally: Siddharth Bakshi, Spyros Lytras, Mohammad Khalid Zakaria. [9]These authors jointly supervised this work: Sam J Wilson, Massimo Palmarini. ✉e-mail: massimo.palmarini@glasgow.ac.uk

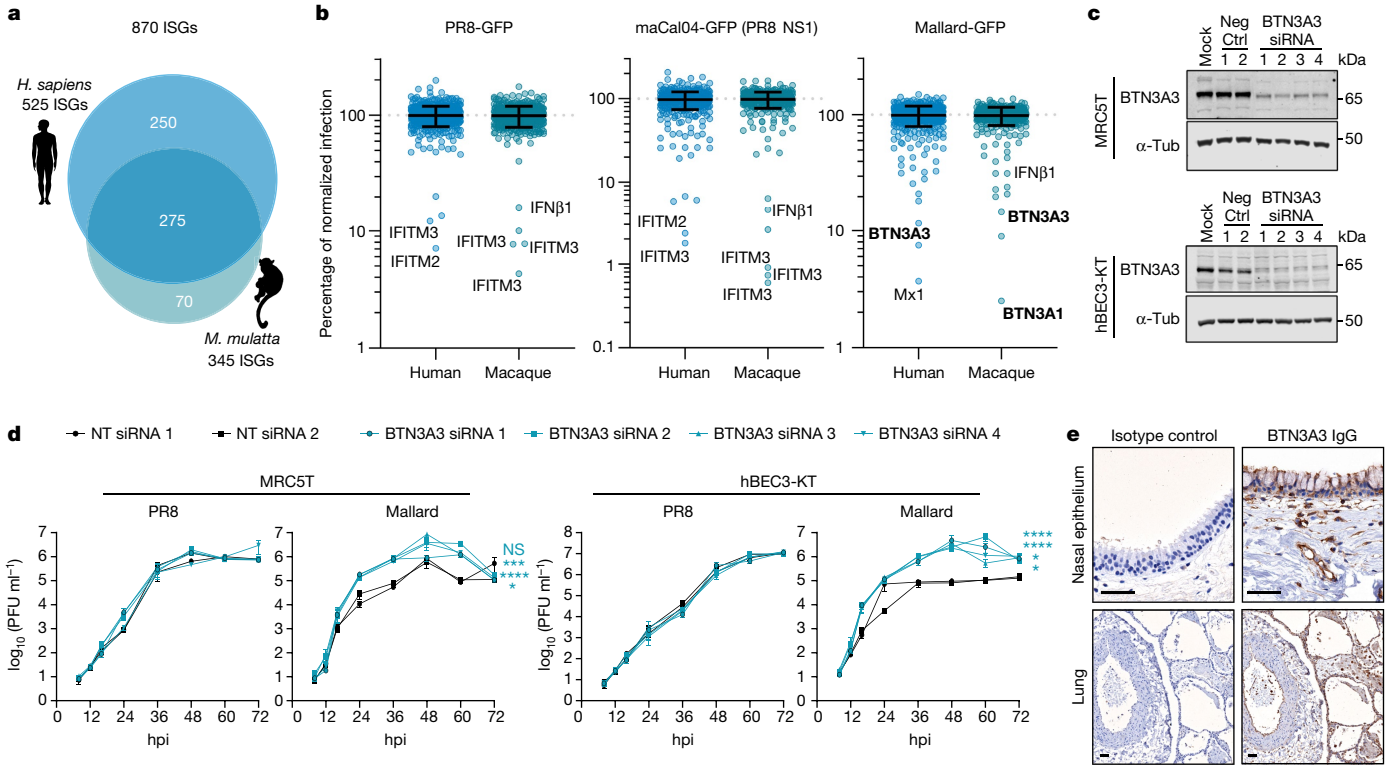

Fig. 1 | BTN3A3 inhibits avian IAVs. a, Schematic representation of the ISG libraries used in the screens. **b**, Graphs showing the results of normalized infections (% median of overall library) of cells expressing individual ISGs with the indicated viruses. ISGs restricting virus replication are labelled (BTN3A3 and BTN3A1 in bold). Each dot represents an individual ISG of libraries illustrated in **a** (870 ISGs in total). **c**, Expression and effective siRNA-driven knockdown of BTN3A3 in MRC5T and hBEC3-KT. Cells were transfected with scrambled (negative control or Neg ctrl) or BTN3A3-targeting siRNAs and protein levels in the resulting cell lysates were assessed by western blot. α-Tubulin was used as loading control. For gel source data, see Supplementary Fig. 1. **d**, Replication kinetics of PR8 and Mallard in siRNA-treated MRC5T and hBEC3-KT. Data are mean ± standard error of the mean (s.e.m.) of three independent experiments (each using two technical replicates). Statistical significance between groups was measured by a two-way analysis of variance (ANOVA). Comparisons were made between area under the curve of the different BTN3A3 siRNA treatment conditions and the average of the two negative controls. NS, not significant, $*P \leq 0.05$, $**P \leq 0.01$, $***P \leq 0.001$, $****P \leq 0.0001$. **e**, Photomicrographs of human nasal epithelium and lung sections subjected to immunohistochemistry. Cells expressing BTN3A3 (shown in brown) are found along the entire nasal epithelium and in endothelial cells and immune cells, as well as pneumocytes. Scale bars, 50 μm.

antiviral properties[20]. Hence, we first aimed to identify human ISGs that contribute to IAV host tropism. We performed arrayed expression screening[21] of 870 human and macaque ISGs (Fig. 1a) using three different green fluorescent protein (GFP)-tagged recombinant IAV strains: A/Puerto Rico/8/1934 (henceforth PR8, a human laboratory-adapted H1N1 strain), A/California/04/2009 (Cal04, a mouse-adapted 2009 pandemic (pdm09) H1N1 strain) and A/mallard/Netherlands/10-Cam/1999 (Mallard, an H1N1 avian strain). These screens (Fig. 1b and Supplementary Table 1) identified ISGs previously shown to be antiviral against IAVs, such as IFITM2, IFITM3 and Mx1 (refs. 11,22–24). Two other ISGs, BTN3A1 and BTN3A3, inhibited the avian virus (Mallard), but not the mammalian viruses (PR8 or Cal04).

To validate these hits, we carried out loss of function experiments. Constitutive expression of BTN3A3 was detected in primary immortalized human foetal lung fibroblasts (MRC5T) and human bronchial epithelial cells (hBEC3-KT) (Fig. 1c). Small-interfering (siRNA)-mediated knockdown of BTN3A3 in these cells resulted in improved replication of the avian Mallard strain, but it did not affect the growth kinetics of PR8 (Fig. 1d). Equivalent knockdown experiments targeting BTN3A1 did not show a significant difference in avian IAVs' replication (Extended Data Fig. 1a,b). By immunohistochemistry, we showed that BTN3A3 is constitutively expressed in the healthy respiratory tract of human donors, both in the upper and lower respiratory tract. BTN3A3 expression was detected in ciliated cells within the nasal epithelium and bronchioli, type I and II alveolar epithelial cells and alveolar macrophages (Fig. 1e). Indeed, available data from human transcriptomic profiles (GTEx consortium) suggest that the lungs have the second highest expression levels of BTN3A3 across 30 tissues analysed (Extended Data Fig. 1c,d). We found that a variety of human lung cell lines showed constitutive expression of BTN3A3, which can then be further upregulated by either type I or type-II IFN (Extended Data Fig. 1e).

The butyrophilin gene superfamily has undergone complex duplication events over its evolutionary history with subfamily three comprising three primate-specific paralogues: BTN3A1, BTN3A2 and BTN3A3 (refs. 2,25). We tested the antiviral activity of overexpressed human BTN3A1, BTN3A2 and BTN3A3 in A549 cells (Fig. 2a). Infection of BTN3-overexpressing cells using GFP-tagged and untagged viruses showed that PR8 was not sensitive to any of the human BTN3 proteins. However, BTN3A1 and BTN3A3 were successful at restricting Mallard (the latter being more effective at restriction) whereas BTN3A2 showed no antiviral effects (Fig. 2b,c). Next, we assessed the antiviral effects of the BTN3 proteins against a wider panel of IAV strains. These included human laboratory-adapted viruses, human clinical isolates and various avian IAVs. None of the human viruses tested were sensitive to any of the BTN3A proteins (Fig. 2d, left panels). However, the replication kinetics of all avian viruses was restricted roughly tenfold by BTN3A1. Restriction of avian viruses by BTN3A3

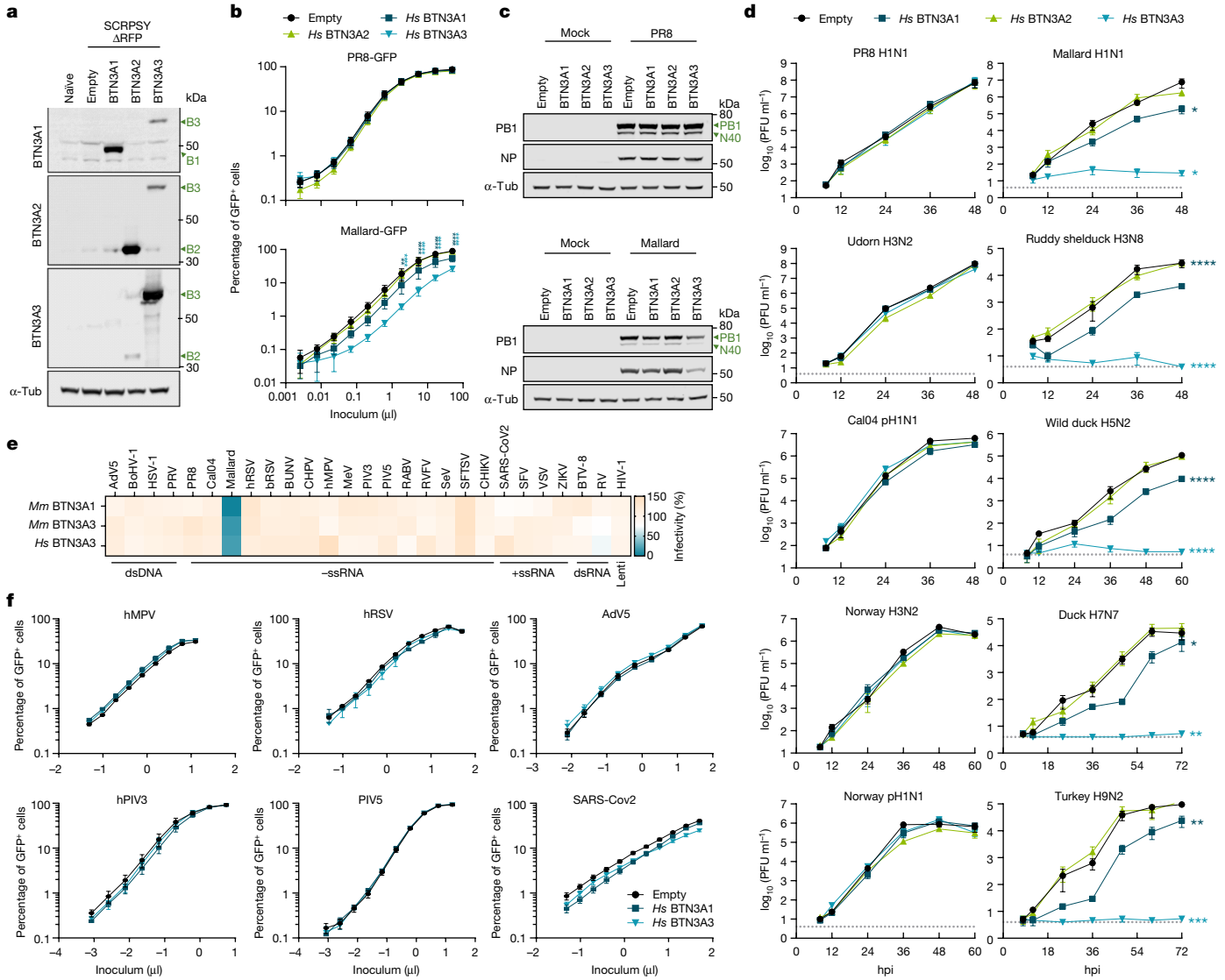

Fig. 2 | Specificity of BTN3s restriction. a, Western blotting of cell lysates obtained from A549 cells stably expressing human BTN3A1 (B1), BTN3A2 (B2) or BTN3A3 (B3). **b**, BTN3-overexpressing A549 cells were challenged with serial dilutions of GFP-tagged PR8 or Mallard for 10 h. On trypsinization and fixation, the percentage of GFP-positive (GFP$^+$) cells was measured by flow cytometry. Data are mean ± s.e.m. of three independent experiments (each using two technical replicates). The multiple comparisons test between each BTN3-expressing and empty control cells was performed using a one-way ANOVA. **c**, BTN3A-expressing A549 cells were infected with PR8 or Mallard WT viruses at MOI 3 for 6 h. Viral protein expression was measured by detection of PB1 (and PB1-N40) and NP by western blot. **d**, Replication kinetics of a panel of human (left panels) and avian (right panels) viruses (MOI, 0.001) in A549-Empty and BTN3A1 or BTN3A3-expressing cells. Data represent mean ± s.e.m. of three independent experiments (each using two technical replicates). Comparisons were made between area under the curve of the different BTN3-expressing and empty cells using a two-way ANOVA. **e**, Heatmap showing normalized infection of cells expressing BTN3A1 and BTN3A3 for a panel of indicated viruses (see Methods for details). **f**, Human BTN3A1 and BTN3A3-overexpressing A549s were challenged with increasing volumes of the indicated GFP-tagged viruses. Cells were fixed at 10 hpi for PR8 and Mallard and 16 hpi for the remaining viruses. Percentage of GFP-positive cells was measured by flow cytometry. Data are mean ± s.e.m. of three independent experiments (each using two technical replicates). Statistical annotations in this figure: $^*P \le 0.05$, $^{**}P \le 0.01$, $^{***}P \le 0.001$, $^{****}P \le 0.0001$. Samples in **a** and **c** were derived from the same experiment and gels were processed in parallel. For gel source data, see Supplementary Fig. 1.

was even greater with viral titres barely reaching the limit of detection and showing a decrease of up to 100,000-fold (Fig. 2d, right panels).

We further tested the antiviral specificity of BTN3A1 and BTN3A3 against an extra 24 viruses, including double-stranded DNA (dsDNA), single-stranded RNA (ssRNA) and double-stranded RNA (dsRNA) viruses. In this screening process, the avian IAV Mallard was the only virus substantially inhibited by BTN3A1 and BTN3A3 (Fig. 2e). Further validation assays against a panel of human respiratory viruses confirmed the specificity of this restriction factor against avian IAVs (Fig. 2f).

BTN3A3 evolution

We then examined the origin of anti-avian IAV activity in the BTN3 gene family. Phylogenetic analysis of the BTN3A genes of the *Haplorrhini* suborder (tarsier, monkeys, apes and humans) indicated that BTN3A1–3 originated through two successive duplications after the split between the new world monkey lineage (*Platyrrhini*) and the old world monkey and ape lineage (*Catarrhini*) around 40–44 million years ago[26] (Extended Data Fig. 2a). Domain detection analysis showed that most BTN3A1 and BTN3A3 genes have a consistent domain organization with one set of N-terminal IgV and IgC domains followed by a PRYSPRY

domain, whereas BTN3A2 genes have lost their PRYSPRY domain (with the exception of *Nomascus leucogenys* BTN3A2) (Extended Data Fig. 2a,b).

Data obtained by transient transduction of A549 cells with BTN3A-expressing lentiviruses followed by viral challenge indicate that the antiviral phenotype of BTN3A3 was gained after the *Platyrrhini-Catarrhini* split, consistent with the two duplication events. Humans, chimpanzees (*Pan troglodytes*), gorillas (*Gorilla gorilla gorilla*), orangutans (*Pongo abelii*), macaques (*Macaca mulatta*) and green monkeys (*Chlorocebus sabaeus*) all have at least one BTN3A1 or BTN3A3 gene capable of inhibiting Mallard viral replication (Extended Data Fig. 3). Our phylogenetic analysis that considers each *Haplorrhini* BTN3 protein domain individually is consistent with previously documented recombination and homogenization of the IgV domain within the BTN3 *Catarrhini* gene subfamily[27] (Extended Data Fig. 4a–d). This incongruence in the evolutionary history of these genes could explain the many gains and/or losses of antiviral function.

We also found that the closest orthologues to BTN3 from mammalian species with endemic IAVs (canine, equine and porcine), the distant galline (*Gallus gallus*) and anatine (*Anas platyrhynchos*) BTN1 orthologues, and other human paralogues of the butyrophilin superfamily did not inhibit PR8 or Mallard, supporting a *Catarrhini* origin of BTN3 antiviral activity (Extended Data Fig. 4e,f).

Determinants of resistance to BTN3A3

To identify viral genetic determinants of BTN3A3 resistance, we engineered 7:1 PR8/Mallard reassortants and tested their ability to form plaques in BTN3A3-overexpressing Madin–Darby canine kidney (MDCK) cells (Extended Data Fig. 5a). All PR8-based reassortants plaqued as efficiently in MDCK-Empty as in MDCK-BTN3A3 cells apart from those containing Mallard segment 5. The converse phenotype was seen in Mallard-based reassortants in which only viruses containing PR8 segment 5 (specifically Mallard 4:4 reassortant encoding PR8 viral ribonucleoprotein (vRNP) components, Mallard 3PNP) formed plaques in MDCK-BTN3A3 cells (Extended Data Fig. 5a). We were unable to rescue the single segment reassortant Mallard 7:1 PR8 Segment 5. Hence, we engineered the reciprocal 7:1 segment 5 reassortants between Mallard and Cal04. We assessed virus fitness in A549-Empty and A549-BTN3A3 cells and confirmed that Mallard segment 5 conferred BTN3A3 sensitivity (Fig. 3a). Segment 5 is monocistronic and encodes the viral nucleoprotein (NP)[28]. To identify the amino acid residue(s) in NP determining the sensitivity or resistance to BTN3A3, we compared the NP sequences of the five human IAVs and five avian IAVs tested in Fig. 2d. Human and avian NP sequences have conserved differences in residues 33, 100, 136, 313, 351, 353 and 357. Of these, positions 33, 100, 313 and 357 have been previously associated with avian-to-human transmission[29]. We rescued PR8 or Mallard single NP mutants and assessed their replication in A549-Empty or A549-BTN3A3. In the PR8 background, we observed no reduction in virus yields in A549-BTN3A3 for any mutants except for PR8 Y313F. Conversely, on a Mallard background the R100V mutant resulted in partial loss of BTN3A3 sensitivity but a near complete evasion was seen for Mallard F313Y (Fig. 3b and Extended Data Fig. 5b). Therefore, we concluded that amino acid residue 313 is a key determinant of BTN3A3 sensitivity and/or resistance.

We next reconstructed a time-calibrated phylogenetic tree from a comprehensive set of more than 30,000 IAV NP amino acid sequences (Fig. 3c). Whereas human NP sequences have almost exclusively 313Y or 313V, all NP clades circulating in avian hosts, as well as the Eurasian avian-like H1N1 swine clade, predominantly show a conserved 313F residue. Less than 1% of avian IAV NP sequences contain 313L, which also confers susceptibility to BTN3A3 (Extended Data Fig. 5b–d). Occurrence of the BTN3A3-resistant 313Y is specific to the human clade, originated from the H1N1 1918 pandemic that subsequently re-assorted into 1957 H2N2 and further 1968 H3N2 pandemic and currently circulates seasonally. Precise dating of the original F313Y change is difficult due to the small number of pre-1918 IAV genomes available. However, recently sequenced genomes from the pandemic all code for NP 313Y[30], suggesting that F313Y took place before or soon after human emergence of the 1918 H1N1 strain.

NP 313V is specific to classical swine H1N1, in which segment 5 entered the human population through reassortment into the 2009 pandemic H1N1. BEAST (Bayesian Evolutionary Analysis Sampling Tree) tip-dating analysis supports a F313V mutation taking place in swine hosts between mid-2002 and the end of 2006 (Extended Data Fig. 6 and Supplementary Discussion). The pdm09 segment 5 is derived from this 313V subclade. We therefore tested whether, similar to PR8, the reversion of NP V313F in pdm09 virus would result in a BTN3A3-sensitive virus. Indeed, unlike its wild-type (WT) counterpart, the mutant Cal04 V313F showed a very pronounced restriction to BTN3A3 (Fig. 3d). Residue 313 had been previously associated with evasion of Mx1 resistance[18,19]. Avian-to-human associated adaptation F313Y, when combined with R100V and/or L283P, shows reduced sensitivity to human Mx1 (ref. 19). However, we observed that the single F313Y mutation, while sufficient to overcome BTN3A3, did not overcome Mx1 restriction (Fig. 3e,f). In addition, loss of function experiments showed that BTN3A3 restriction occurs in an Mx1-independent manner (Extended Data Fig. 7a,b).

We further validated the role of NP residue 313 as a determinant of resistance to BTN3A3 in an in vivo experimental model. B6 mice were intranasally transduced with adeno-associated virus (AAV) vectors (AAV6.2FF) expressing either GFP (negative control) or BTN3A3, and subsequently infected with Cal04 WT or V313F mutant re-assorted to express PR8 glycoproteins to maximize replication in mouse tissues (6:2 PR8 HA,NA; a reassortant formed by the internal proteins of PR8 and the external haemagglutinin (HA) and neuraminidase (NA) glycoproteins of Cal04)[31]. AAV vectors achieved efficient expression of GFP and BTN3A3 in the mouse respiratory tract 3 weeks after transduction (Fig. 3g). In challenged mice, Cal04 (6:2 PR8 HA,NA,) WT fitness in the lungs was not significantly impaired in BTN3A3-expressing mice compared to controls. Conversely, titres reached by the single mutant V313F in BTN3A3-expressing mice were significantly lower than those reached in GFP-expressing mice (Fig. 3h), indicating that BTN3A3 restriction can also occur in vivo.

Mechanisms of BTN3A3 restriction

NP is an essential protein in the IAV life cycle with the primary function of encapsidating the viral genome to ensure effective RNA transcription, replication and packaging[32]. As well as being a structural RNA-binding protein, NP is also a key adapter between virus and host cell processes as it is essential for the nuclear or cytoplasmic trafficking of vRNPs[32–34]. Hence, to test whether BTN3A3 inhibits vRNP nuclear import we performed synchronized infections of A549-Empty or A549-BTN3A3 cells followed by nuclear and/or cytoplasmic fractionation at early time points after infection. At 45 minutes post infection, levels of Mallard vRNP-containing proteins in both cytoplasmic and nuclear fractions were equal between A549-Empty and BTN3A3-expressing cells, suggesting equally efficient virus entry and vRNP nuclear import (Fig. 4a top panel, and related quantification presented in Extended Data Fig. 7c). At 90 min post infection, by which point initial transcription and translation of viral genes had resulted in an increase of viral protein, a difference in viral protein levels was seen between the two cell lines in both cytoplasmic and nuclear fractions (Fig. 4a middle panel, Extended Data Fig. 7c). This difference was further amplified at 6 hours post infection (hpi) (Fig. 4a bottom panel and Extended Data Fig. 9). Hence, these data indicate that the initial stages of the virus life cycle, including binding, entry and vRNP nuclear import were largely unaffected by BTN3A3 overexpression whereas subsequent steps could be affected.

To investigate this further, we measured RNP-driven viral transcription and/or replication and translation using RNP reconstitution

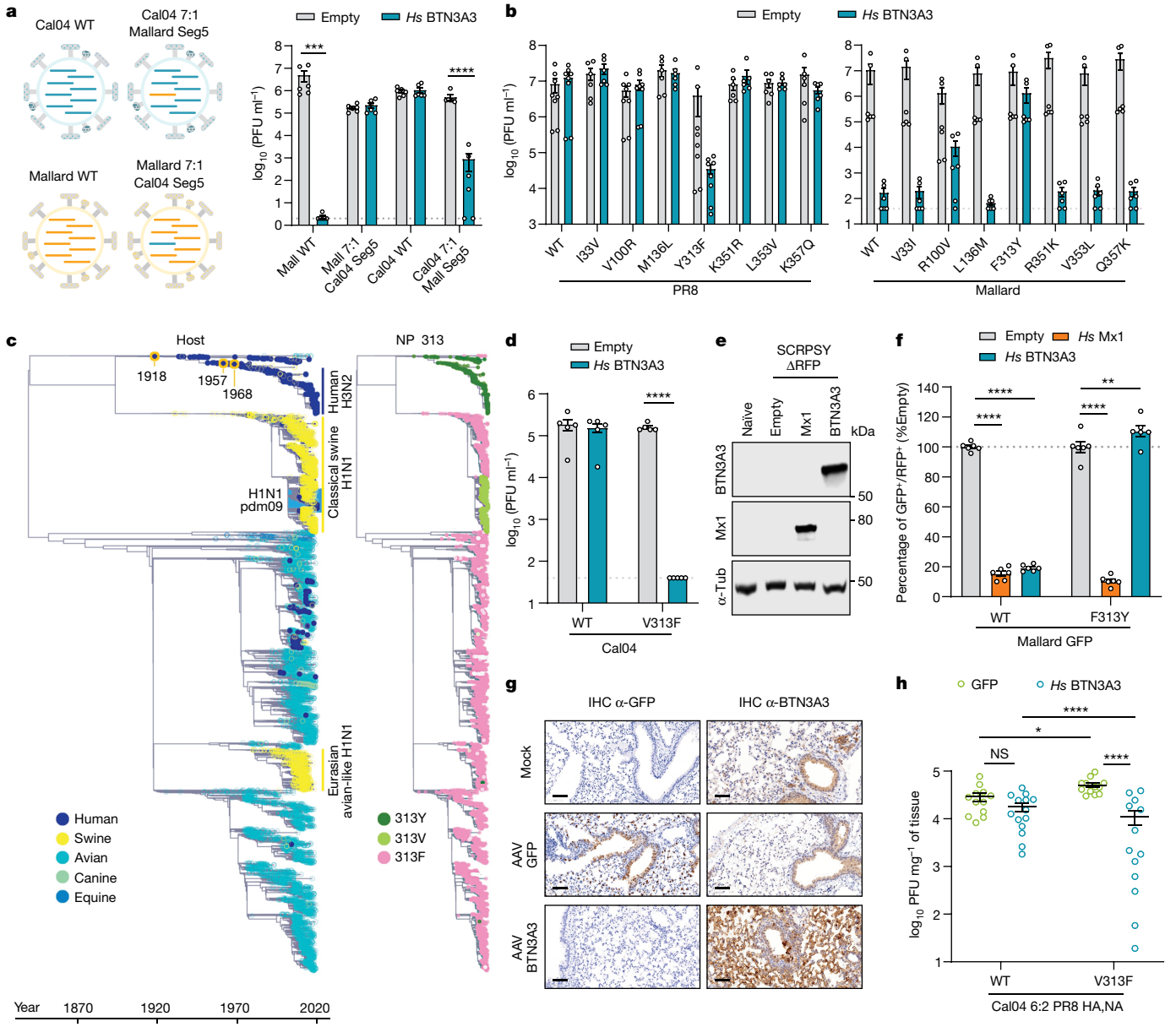

Fig. 3 | Determinants of BTN3A3 sensitivity. a, A549-Empty and BTN3A3-expressing cells were infected for 48 h with the schematized viruses (left, MOI 0.001), after which infectious titres were quantified by plaque assays (right). Data are mean ± s.e.m. of three independent experiments (each using two technical replicates). The multiple *t*-tests were performed using the Holm–Šídák method. **b**, PR8 and Mallard NP single mutants were used to infect A549-Empty and A549-BTN3A3 and titrated as in **a**. **c**, Tip-dated maximum likelihood phylogeny of the filtered IAV NP-coding sequence dataset (Methods). Tip shapes are annotated by host (left) and 313 residue (right). Legend only shows residues occurring in more than 5% of the sequences. **d**, Cal04 WT and V313F mutant were used to infect A549-Empty and A549-BTN3A3. Virus quantification and statistical analysis were performed as in **a**. **e**, Western blotting of cell lysates obtained from A549 cells stably expressing human Mx1 or BTN3A3. Samples were derived from the same experiment and gels were processed in parallel. For gel source data, see Supplementary Fig. 1. **f**, A549 overexpressing human Mx1 and BTN3A3 were infected with GFP-tagged Mallard WT or F313Y. Ten hpi cells were trypsinized, fixed and RFP- and GFP-positive cells were measured by fluorescence-activated cell sorting. Data are mean ± s.e.m. from three independent experiments (each using two technical replicates). Statistical differences were calculated as in **a**. **g**, C57BL/6 mice were inoculated with PBS (mock), AAV-GFP or AAV-BTN3A3 for 3 weeks after which lungs were examined for GFP and BTN3A3 expression. Scale bars, 70 µm. **h**, Three weeks after AAV-GFP or AAV-BTN3A3 treatment, mice were infected with Cal04 (6:2 PR8 HA,NA) WT or V313F mutant. Lung viral titres were assessed 3 days post infection. Data represent mean ± s.e.m. Each group included 12 to 14 mice. Dots represent individual mice. Source data are available in Supplementary Table 9. Multiple comparisons were performed from a one-way ANOVA. Statistical annotations in this figure are defined as $^{*}P \leq 0.05$, $^{**}P \leq 0.01$, $^{***}P \leq 0.001$, $^{****}P \leq 0.0001$.

minireplicon reporter assays. Using either viral RNA (vRNA)- or cRNA complementary RNA (cRNA)-like reporter constructs, the transcription and/or replication activities of NP 313F-coding RNPs were significantly reduced in BTN3A3-overexpressing cells (Fig. 4b,c and Extended Data Fig. 8). In principle, this could be due to effects on viral transcription, replication, translation or protein stability.

To examine the effects of BTN3A3 in viral primary transcription, A549-Empty and A549-BTN3A3 cells were pretreated with cycloheximide (CHX, a translation elongation inhibitor) and subsequently infected with Mallard WT or the F313Y mutant. Viral messenger RNA was left to accumulate for 12 h, RNA was extracted and protein synthesis from viral mRNA was measured using a rabbit reticulocyte lysate

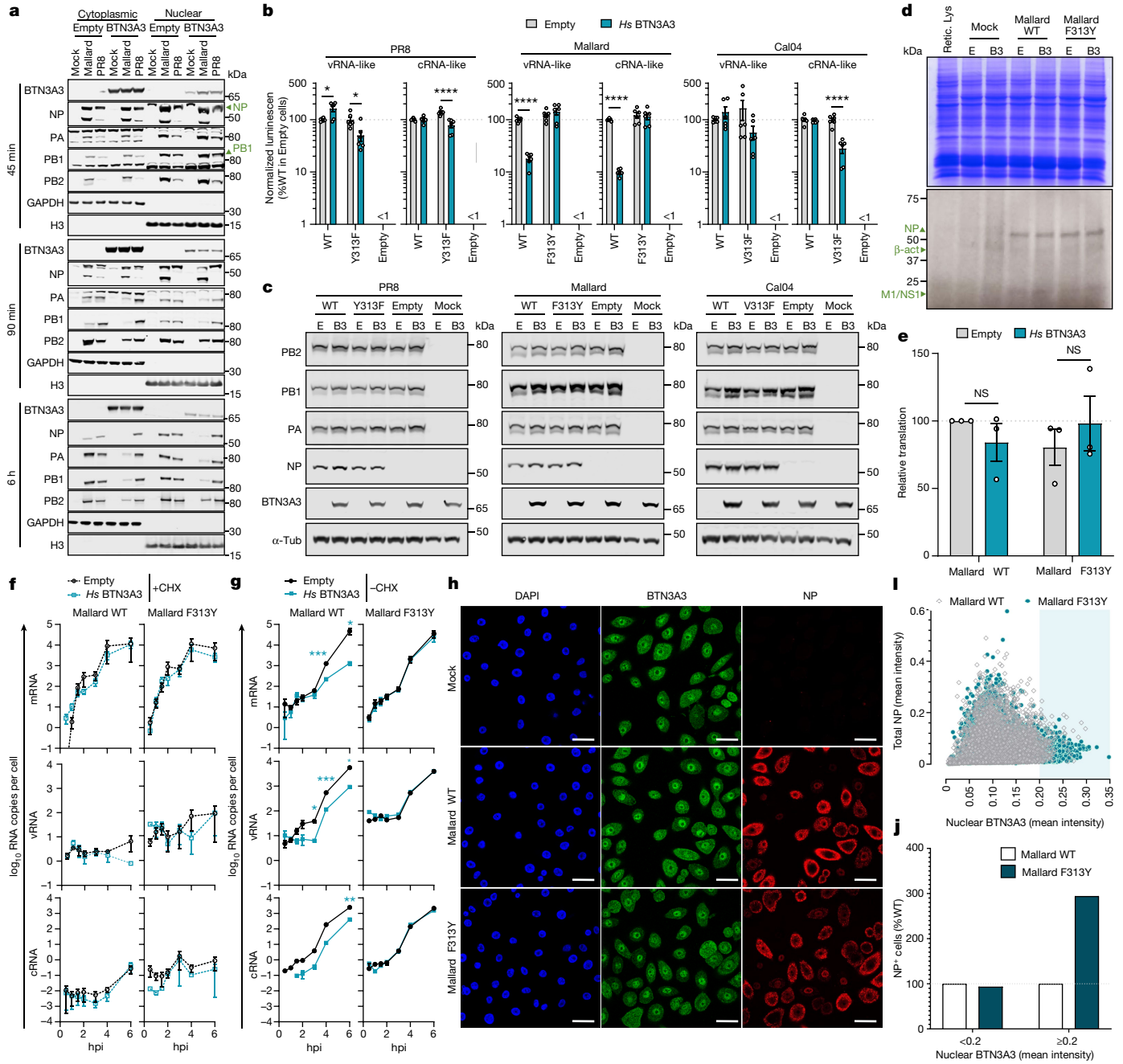

Fig. 4 | BTN3A3 blocks vRNA transcription. a, A549-Empty and A549-BTN3A3 cells were infected with PR8 and Mallard WT (MOI 3). Following nuclear and/or cytoplasmic fractionation, vRNP components and cellular markers were detected by western blotting. **b**, Minireplicon assays in 293T-Empty and 293T-BTN3A3 cells of the indicated viruses alongside luciferase-based vRNA- or cRNA-like reporter and transfection control plasmids. 48 h after transduction, luminescence was measured. Values were normalized to WT NP-coding RNPs in 293T-Empty cells. Data are mean ± s.e.m. of three independent experiments (each using two technical replicates). **c**, Protein expression of RNP components from 293T-Empty (E) and 293T-BTN3A3 (B3) cells transfected as in **b** were assessed by western blot. **d**, A549-Empty and A549-BTN3A3 cells were pretreated with CHX and infected at an MOI of 3. Twelve hpi, total RNA was extracted and equivalent volumes were used in in vitro translation assays. The top panel represents Coomassie staining as loading control. The bottom panel exemplifies autoradiography detection. **e**, Densitometry quantification of NP (translated from segment 5 mRNA) from autoradioactive gels. Data are mean ± s.e.m. of three independent experiments and are normalized to Mallard WT in A549-Empty cells. **f**,**g**, A549-Empty and A549-BTN3A3 cells were treated (**f**) or untreated (**g**) with 100 μg ml^{-1} CHX and infected at an MOI of 3. vRNA species were quantified by a two-step RT–qPCR at indicated time points. Data are mean ± s.e.m. of three (vRNA and cRNA) or four (mRNA) independent experiments. **h**, Representative image of confocal microscopy of hBEC3-KT cells infected with Mallard WT or F313Y at an MOI of 3. At 6 hpi, cells were immunostained for NP and BTN3A3 (nuclei in blue). Scale bar, 35 μm. **i**, Quantification of total NP and nuclear BTN3A3 intensities for Mallard WT and F313Y. The data constitute single data points of more than 3,500 cells from four independent experiments. **j**, Values from **h** were stratified on the basis of nuclear BTN3A3 intensity. The data represent the relative abundance of total infected cells in each nuclear BTN3A3 intensity ranges. Values were normalized to Mallard WT. Statistical analyses in this figure are the result of several *t*-tests between Empty and BTN3A3 conditions and were performed using the Holm–Šídák method. Annotations are defined as $^{*}P \le 0.05$, $^{**}P \le 0.01$, $^{***}P \le 0.001$, $^{****}P \le 0.0001$. Samples in **a** and **c** were derived from the same experiment and gels were processed in parallel. For gel source data, see Supplementary Fig. 1.

system. For both Mallard WT and Mallard F313Y, autoradiography analysis revealed equal levels of the main viral proteins between A549-Empty and A549-BTN3A3 cells (Fig. 4d,e), suggesting that viral primary transcription was not inhibited by BTN3A3.

We next tested whether RNP replication activity was impaired by BTN3A3 using quantitative PCR (qPCR) assays to measure viral mRNA, vRNA and cRNA species at early time points after infection in the presence or absence of CHX. The ablation of protein synthesis by CHX results in the abrogation and/or inhibition of IAV genome replication activity that is dependent on newly synthesized NP monomers[35]. Therefore, new vRNA and cRNA synthesis was fully inhibited by CHX (Fig. 4f, middle and bottom panels). Consistent with observations in Fig. 4d,e, in the presence of CHX, Mallard WT mRNA levels were not affected by BTN3A3 (Fig. 4f, top panels). In CHX-untreated cells, Mallard WT mRNA levels were insensitive to BTN3A3 in the first 3 hpi, but thereafter were reduced, by nearly 100-fold at 6 hpi. Potentially explaining this late difference in viral mRNA synthesis, BTN3A3 overexpression both reduced and delayed vRNA and cRNA accumulation in Mallard WT-infected cells. By contrast, the BTN3A3-resistant mutant Mallard F313Y showed no differences in the synthesis of any vRNA species between infected A549-Empty and A549-BTN3A3 cells (Fig. 4f,g, right halves). Collectively, these data indicate that BTN3A3 restricts sensitive IAVs mainly at the level of viral genome replication.

IAV RNA synthesis takes place in the nucleus, and despite BTN3A3 having been described as a transmembrane protein, localization of constitutively expressed BTN3A3 in hBEC3-KT cells was predominantly nuclear (Fig. 4h). In these cells, we also found components of the RNP complex, of both avian IAVs and mammalian IAVs, could also be coimmunoprecipitated with BTN3A3 (Extended Data Fig. 9). Image analysis of infected hBEC3-KT cells showed that, when cells express high levels of nuclear BTN3A3, viral protein synthesis (measured by NP accumulation) of Mallard WT was weaker (Fig. 4i,j). Furthermore, NP accumulation from a BTN3A3-resistant mutant was less sensitive to high levels of nuclear BTN3A3. Similar observations were made for Cal04 WT (BTN3A3 resistant) and the BTN3A3-sensitive mutant Cal04 NP V313F (Extended Data Fig. 10).

Virus genotype of zoonotic avian IAVs

We next analysed whether BTN3A3 evasion could be correlated with the zoonotic potential of avian IAVs. We focused on avian H7N9 given the high numbers of spillover events caused by these viruses. The NP of H7N9 contains a 313F residue and so theoretically should be restricted by BTN3A3. However, the high number of human infections caused by H7N9, led us to propose that they overcome BTN3A3 restriction through an alternative mechanism. We tested a 6:2 H7N9 reassortant (containing the glycoproteins from PR8 and the internal segments from H7N9) in A549-Empty and A549-BTN3A3 cells. The reassortant H7N9 was poorly restricted by BTN3A3, despite possessing a 313F-coding NP, whereas a 6:2:1 H7N9 reassortant containing Mallard NP was restricted roughly 70-fold on average (Fig. 5a). Comparison of H7N9 and Mallard NP sequences highlighted differences at eight amino acid residues (positions 34, 52, 186, 352, 373, 377, 406 and 482). To determine whether any of these amino acid substitutions enabled H7N9 viruses to evade BTN3A3 restriction, we constructed and tested single amino acid mutants, and identified that the NP substitution N52Y rendered H7N9 sensitive to BTN3A3 (Fig. 5a). The effect of 52N was only seen in the presence of 313F; the Y52N mutation was not sufficient to confer BTN3A3 sensitivity in the presence of 313Y (Fig. 5b).

The 52N-coding NP sequences occur in several independent avian IAV sublineages. Most of all, using time-calibrated phylogenetic analysis, we identified an initial switch of NP 52Y to 52N that we estimated occurred between August 1999 and October 2001 and that over time became dominant in the avian H9N2 and the H7N9 lineages from which all human H7N9 epidemic virus NPs have originated (Fig. 5c).

To further explore the importance of NP residue at position 52, we analysed its polymorphism across all strains of IAVs. Avian IAVs predominantly encode NP 52Y with 25% of the isolates coding for 52N or 52H (Fig. 5d, left). Swine IAVs almost universally contain NP 52Y whereas equine and canine NP sequences present the most 52H. Human-derived IAV possess either 52Y or 52H in broadly equal parts (Fig. 5d, left). The substantial prevalence of 52Y in human IAVs can be explained by the co-occurrence of NP 313Y, which provides resistance to BTN3A3 and is dominant over 52Y (Fig. 5b). Analysis of all subtypes of avian IAV NP sequences obtained from humans (representing spillover events) showed not only the most 52N in H3, H6, H7, H9 and H10 subtypes, but also less frequent residues 52Q, 52H and 52Y sidechains (Fig. 5d, right, and Supplementary Table 2), with the last almost universally in the H5 subtype. We show that mutants engineered with 52Q or 52H in either the Mallard or H7N9 backgrounds result in BTN3A3 evasion as efficiently as those possessing 52N (Fig. 5e). Despite being separated in the primary sequence of NP, positions 52 and 313 are closely juxtaposed within the NP head domain (Fig. 5f). Moreover, both residues are located on the surface of the NP trimer, indicating that they would be accessible to interactions with other viral and host factors when NP oligomerizes to form positive-sense complementary RNP and/or vRNP.

It is important to note that NP residue 52 has been also implicated in the evasion of Mx1 resistance[19,20]. However, by overexpression of BTN3A3 or Mx1, we determined that IAV sensitivity and/or resistance to these restriction factors showed differential dependence on NP residues 52 and 313 (Extended Data Fig. 11a). The evasion of BTN3A3 restriction conferred by residue 52 is dependent on residue 313, which is not the case for evasion of Mx1 restriction. A correlation in human patients between disease severity induced by H7N9 and certain human MX1 alleles has also been described in genome-wide association studies[36]. Incidentally, BTN3A3 is very conserved in humans (Supplementary Table 3) and we found no specific association with severe disease and BTN3A3 alleles using the same genome-wide association analyses (Extended Data Fig. 11b,c).

In summary, a BTN3A3-sensitive viral genotype can be defined as possessing NP-coding 313F and 52Y whereas BTN3A3-resistant viruses have NP 313Y/V and/or 52N/H/Q. Of the roughly 1,700 avian IAV sequences detected in human patients, 77% have a BTN3A3-resistant genotype, whereas the remaining 23% are BTN3A3-senstive. The last belong virtually all to highly pathogenic avian influenza H5N1 (308 of 309 sequences; Extended Data Fig. 12a). Using 7:1 PR8-based reassortants, we experimentally confirmed that viruses harbouring H5N1 NP sequences with a predicted BTN3A3-sensitive genotype were indeed restricted in A549-BTN3A3 cells (Extended Data Fig. 12b). Also, 99.5% of BTN3A3-resistant viruses isolated from human patients originated from low pathogenic avian influenza lineages.

Frequency of BTN3A3-resistant avian IAVs

We next examined how the frequency of the BTN3A3-resistant genotype changed over time in avian IAVs circulating in birds, including those involved in major epizootic events. Analysis of the frequency of BTN3A3-resistant genotype among IAV isolates from birds (roughly 29,000 sequences from the Global Initiative on Sharing All Influenza Data (GISAID) EpiFlu database; Supplementary Table 4) showed a peak between 2012 and 2019, fluctuating from 49.5 to 62%. This correlates with peaks of avian-to-human IAV zoonotic cases within the same time period (Fig. 5g, first panel).

Avian H9N2 viruses represent the serotype with the highest percentage of BTN3A3-resistant genotype, having reached a maximum of 97% in 2018, along with a high number of detected sequences (Fig. 5g, second panel). The H9N2 G57 genotype is highly promiscuous and is regarded as a main donor of viral internal genes that resulted in viruses spilling over into humans[37]. Through reassortment events, before 2013, H9N2 gave its internal gene segments to the newly emerging H7N9 strain.

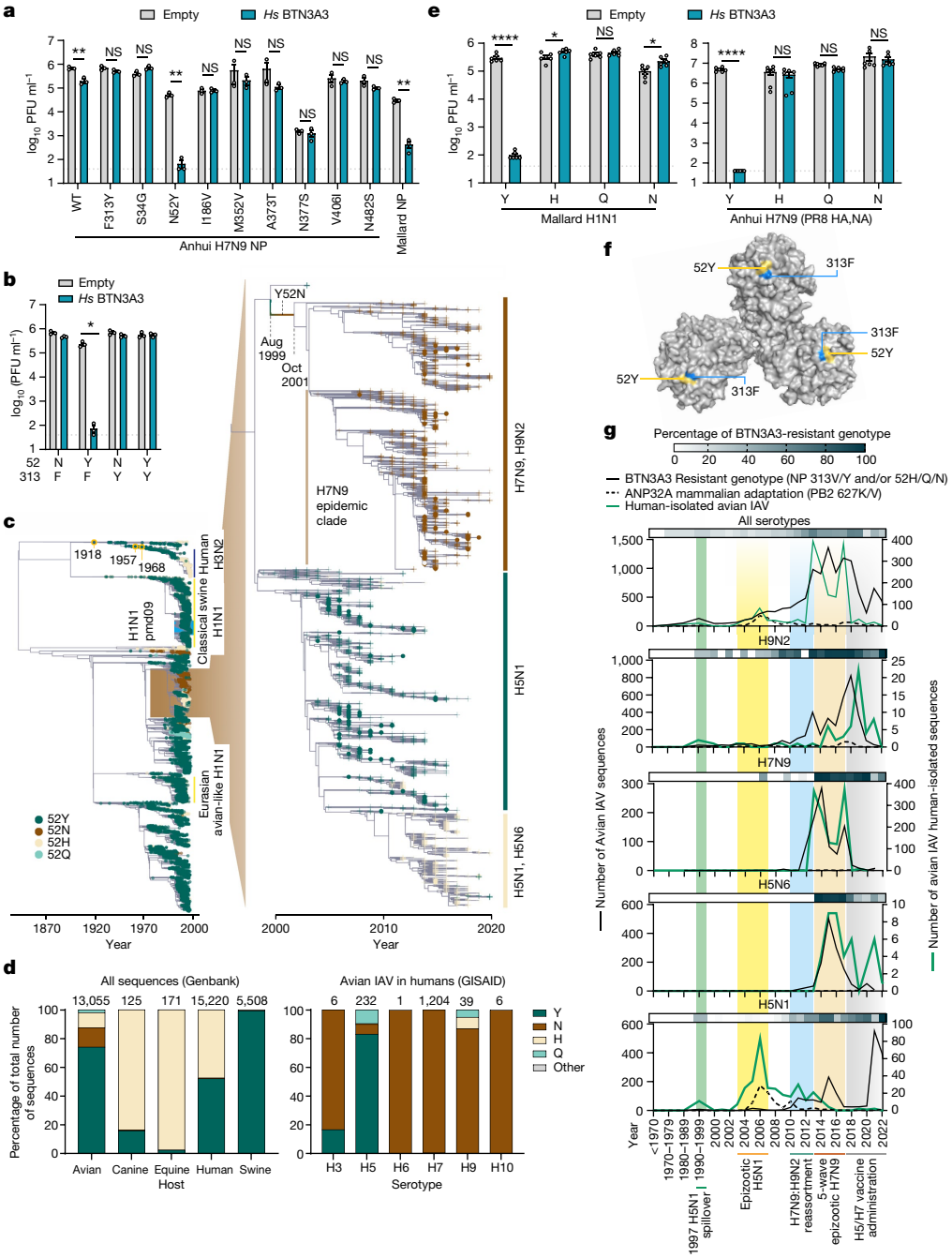

Fig. 5 | Evasion of BTN3A3 by zoonotic avian IAVs. a,**b**, Replication of H7N9 (6:2 PR8 HA,NA) reassortant viruses with the indicated single (**a**) or double (**b**) NP mutations in A549-Empty or A549-BTN3A3 cells. Cells were infected at an MOI of 0.001 for 48 h and viruses titrated by plaque assay. Data are mean ± s.e.m. from three independent experiments (each using two technical replicates). Several *t*-tests were performed using the Holm–Šídák method. **c**, Tip-dated maximum likelihood phylogenies of the filtered IAV NP-coding sequence dataset (left) and of all sequences clustering within the highlighted avian IAV clade (right). Tip shapes are coloured by site 52 residues (only residues present in more than 1% of the sequences are shown in the legend). On the right, human isolates are annotated with circles and non-human isolates are annotated with transparent crosses to highlight human transmission. The branch where the Y52N change took place is annotated on the tree. Serotypes present in more than 10% of the sequences in each subclade are shown on the right. **d**, Identity of amino acid residue in position 52 of all NP proteins available in the NCBI Flu dataset used in this study (Methods) (left) or in those collected from spillovers of avian IAVs in humans (GISAID) (right). Numbers over the bars indicate the number of sequences. **e**. Infectious virus titres obtained in A549-Empty and BTN3A3-expressing cells with NP 52 mutants of either Mallard or H7N9 6:2 PR8. Cells were infected at an MOI of 0.001 for 48 h and viruses titrated by plaque assay. Data are mean ± s.e.m. from three independent experiments (each using two technical replicates; statistical analysis performed as in **a** and **b**). **f**, Surface structure of trimeric NP (residues 52 and 313 are highlighted). **g**, Chronological association between the accumulation of the BTN3A3-resistant genotype and PB2 627K/V in IAVs circulating in avian species or isolated from human patients. Statistical annotations in this figure are defined as $*P \le 0.05$, $**P \le 0.01$, $***P \le 0.001$, $****P \le 0.0001$.

Consequently, whereas H9N2 human isolates have been detected sporadically since 1999, H7N9 was first detected in humans in 2013, resulting in a five-wave epidemic event lasting until 2018 (Fig. 5g, third panel). Moreover, of all avian-isolated H7N9 sequences deposited in GISAID (the Global Initiative on Sharing All Influenza Data) before 2013, only 14% (seven out of 50) show a BTN3A3-resistant genotype (conferred

by NP 52H). By contrast, from 2013 onwards, 93.5% of H7N9 (n = 849) show a BTN3A3-resistant genotype that is instead conferred by the H9N2 G57-descendant NP 52N.

In addition to H7N9, another example of a G57-segment containing virus is the HPAI H5N6 with its first human infection being detected in 2014 (ref. 38), reaching a peak of human infections in 2015–2016. Like the H7N9 epizootic event, the chronology of acquisition of BTN3A3 resistance correlates with H5N6 avian-to-human spillovers (Fig. 5g).

For comparative purposes, we also analysed PB2 amino acid 627, as it is well reported that viruses harbouring 627K (or 627V) have a replicative advantage in human cells as they are better supported by human ANP32A than the avian counterpart 627E[15]. In the analysed dataset, roughly 63% of all avian IAVs isolated in human patients possess a PB2 627K/V compared to a frequency of roughly 3% in viruses circulating in birds. Specifically in the 2013-2018 H7N9 epizootic waves, 74% of viruses isolated from human patients possessed a PB2 627K/V. However, very few avian H9N2, H7N9 and H5N6 circulating in birds harboured the 'mammalian'-adapted PB2 627K/V before, during or after zoonotic events. These data indicate that BTN3A3 resistance is important for spillover whereas the acquisition of 627K/V is selected in humans infected with avian IAVs.

As described above, the HPAI H5N1 spillover events do not show overall an association with a BTN3A3-resistant genotype. It is, however, interesting to note that ten out of ten sequences publicly available from the first outbreak caused by H5N1 in 1997 in Hong Kong[39] show a BTN3A3-resistant genotype. In addition, although the number of sequences available from H5N1 circulating in birds from the same period and location are relatively low (n = 8), they also all possess a BTN3A3-resistant genotype. Another interesting observation is associated with the waterfowl-origin A/Goose/Guangdong/1/96 (GsGd) lineage of HPAI H5N1 viruses that re-emerged in China in 2003 (ref. 40). Unlike H9N2, H7N9 and H5N6, avian isolates of HPAI H5N1 showed a high frequency of the PB2 627K residue, in roughly the same period when an increased number of sequences of zoonotic cases caused by these viruses was observed (Fig. 5g, lower panel).

Discussion

Our study reveals that human BTN3A3 is a powerful barrier for the replication of avian IAVs but not human IAVs. Through data obtained in vitro in cell culture assays and in vivo in experimental animal models, in addition to comprehensive evolutionary analyses, we showed that evasion of human BTN3A3 is one of the risk factors for the zoonotic potential of IAVs. To date, avian subtypes H5, H7, H9 and, less often, H3, H6 and H10, have spilled over and caused human infections[7,41].

Butyrophilins were discovered originally as proteins involved in lactation and milk production, but they are also known to have immunomodulatory functions[2,42–44]. This group of proteins have not been generally associated with antiviral properties, although one of two studies using ISG libraries against Ebola virus replicons identified BTN3A3 as a restriction factor for this virus[45,46]. The anti-avian IAV properties of BTN3A3 arose in primates. Hence, humans are the only species maintaining endemic infections with influenza viruses that restrict avian IAV replication through this effector. Neither avian species nor swine impose a BTN3A3-related selective pressure on the NP 313 residue.

We showed that BTN3A3 interferes mostly with avian IAV vRNA replication, at the early stages of the virus life cycle after the entry of the vRNP complex into the nucleus and primary vRNA transcription.

There are several independent lines of evidence pointing to evasion of BTN3A3 as a key risk factor for the zoonotic potential of IAVs. First, all the human endemic IAV viruses, including those that emerged in 1918, are resistant to BTN3A3. Second, the swine H1N1 2009 pandemic virus originated from a BTN3A3-resistant NP 313V clade that we estimate appeared in pigs between 2002 and 2006, ahead of the start of the 2009 pandemic (Extended Data Fig. 6). Third, evasion of BTN3A3 restriction is a conserved trait of most avian viruses that have successfully spilled over into humans, due to a mutation from a BTN3A3-sensitive 52Y residue to a BTN3A3-resistant N, Q or H residue (or very rarely in H3N8 through the F313V mutation) and further propose that residue 52 masks the effect of 313F[3]. Finally, we showed that avian IAVs circulating in birds showed an increased frequency of the BTN3A3-resistant genotype in 2011–2012, ahead of the initial H7N9 outbreak in humans. Indeed, it is only around 2013, when the first human H7N9 cases were identified, that the NP 52N residue became dominant in this lineage.

There are many barriers preventing zoonotic cross-species transmission of animal IAVs, and BTN3A3 has to be considered one of many rather than the sole determinant of the zoonotic potential of IAVs. Mx1 is another restriction factor for avian IAVs. The NP residues 313 and 52 that are critical in BTN3A3 evasion/resistance have also been associated with Mx1 resistance[18,19]. We presented in vitro data indicating that, despite affecting similar stages of the virus life cycle and through common amino acid residues, BTN3A3 acts independently from Mx1. Moreover, our in vivo experiments were carried out in regular C57BL/6 mice that, like many other laboratory mouse strains, possess a non-functional Mx1 (refs. 47,48), further reinforcing the point that BTN3A3 acts in an Mx1-independent manner. It is also interesting to note a recent study suggesting that IAV NP regulates mitophagy and the Y313F mutation attenuates this process[49]. Hence, at least two independent human restriction factors target a conserved surface of NP, suggesting that this constrained region is a key determinant of the zoonotic potential of avian IAVs.

The exception to the rule of BTN3A3 representing a key barrier to avian IAV spillover into humans is represented by highly pathogenic H5N1. HPAI viruses are defined by the presence of a polybasic cleavage sites in their haemagglutinin protein that may allow the virus a wider cellular tropism, potentially providing the ability to infect BTN3A3 low-expressing cells, or a more efficient replication fitness leading to a higher chance of a successful infection[50] and therefore overriding the antiviral effects of BTN3A3. Notably, only around 30% of H5N1 isolated from humans possess the adaptive PB2 627K mutation, as opposed to more than 70% of all the other avian viruses that successfully spilled over into humans. Hence, HPAI H5N1 viruses appear to be able to infect humans in the absence of either a BTN3A3-resistant genotype or PB2 human adapting mutations. These observations suggest that this virus may possess distinctive features that allow it to spill over in humans more effectively than other avian viruses.

In recent years, the GsGd lineage of HPAI H5 virus that originally emerged in Asia, has caused an increasing number of outbreaks in wild birds, poultry and wild mammals across several continents[51]. This lineage shows a high frequency of the BTN3A3-resistant genotype. Of note, is a particularly concerning recent outbreak of H5N1 in a farm housing roughly 50,000 mink in Spain[52]. Viruses isolated from this outbreak showed both an ANP32A-linked PB2 T271A mutation, associated with enhanced polymerase activity in mammalian cells[53], and a NP 52N mutation conferring a BTN3A3-resistant genotype that was acquired in an avian host before emergence of the H5N1 virus in mink[52]. Transmission of these viruses within farmed animal populations provide them with the opportunity to further adapt to the mammalian host, in addition to provide further opportunities for onwards transmission to humans. Hence, H5N1 viruses with a BTN3A3-resistant genotype may be better posed in the future to adapt to humans.

Global efforts during the SARS-CoV-2 pandemic and over the years for IAV infections have shown that surveillance based on virus genomic sequences can be a useful tool not only to provide insight into disease spread and epidemiology, but also for the early identification of viruses with undesirable phenotypic traits from a public health perspective. The BTN3A3-resistant genotype is one of the determinants associated with avian IAV spillover in humans that should be considered in risk-assessment frameworks[54].

Online content

Any methods, additional references, Nature Portfolio reporting summaries, source data, extended data, supplementary information, acknowledgements, peer review information; details of author contributions and competing interests; and statements of data and code availability are available at https://doi.org/10.1038/s41586-023-06261-8.

1. Lipsitch, M. et al. Viral factors in influenza pandemic risk assessment. *eLife* https://doi.org/10.7554/eLife.18491 (2016).
2. Afrache, H., Gouret, P., Ainouche, S., Pontarotti, P. & Olive, D. The butyrophilin (BTN) gene family: from milk fat to the regulation of the immune response. *Immunogenetics* **64**, 781–794 (2012).
3. Ye, Q., Krug, R. M. & Tao, Y. J. The mechanism by which influenza A virus nucleoprotein forms oligomers and binds RNA. *Nature* **444**, 1078–1082 (2006).
4. Yoon, S.-W., Webby, R. J. & Webster, R. G. in *Influenza Pathogenesis and Control* Vol. I (eds W. Compans, R. A. & Oldstone, M. B. A.) 359–375 (Springer International Publishing, 2014).
5. Krammer, F. et al. Influenza. *Nat. Rev. Dis. Primers* **4**, 3 (2018).
6. Harrington, W. N., Kackos, C. M. & Webby, R. J. The evolution and future of influenza pandemic preparedness. *Exp. Mol. Med.* **53**, 737–749 (2021).
7. Short, K. R. et al. One health, multiple challenges: the inter-species transmission of influenza A virus. *One Health* **1**, 1–13 (2015).
8. Liu, D. et al. Origin and diversity of novel avian influenza A H7N9 viruses causing human infection: phylogenetic, structural, and coalescent analyses. *Lancet* **381**, 1926–1932 (2013).
9. Wang, X. et al. Epidemiology of avian influenza A H7N9 virus in human beings across five epidemics in mainland China, 2013–17: an epidemiological study of laboratory-confirmed case series. *Lancet Infect. Dis.* **17**, 822–832 (2017).
10. Liu, W. J. et al. Avian influenza A (H7N9) virus: from low pathogenic to highly pathogenic. *Front. Med.* **15**, 507–527 (2021).
11. Long, J. S., Mistry, B., Haslam, S. M. & Barclay, W. S. Host and viral determinants of influenza A virus species specificity. *Nat. Rev. Microbiol.* **17**, 67–81 (2019).
12. Rogers, G. N. & Paulson, J. C. Receptor determinants of human and animal influenza virus isolates: differences in receptor specificity of the H3 hemagglutinin based on species of origin. *Virology* **127**, 361–373 (1983).
13. Di Lella, S., Herrmann, A. & Mair, C. M. Modulation of the pH stability of influenza virus hemagglutinin: a host cell adaptation strategy. *Biophys. J.* **110**, 2293–2301 (2016).
14. Zaraket, H. et al. Increased acid stability of the hemagglutinin protein enhances H5N1 influenza virus growth in the upper respiratory tract but is insufficient for transmission in ferrets. *J. Virol.* **87**, 9911–9922 (2013).
15. Long, J. S. et al. Species difference in ANP32A underlies influenza A virus polymerase host restriction. *Nature* **529**, 101–104 (2016).
16. Blumenkrantz, D., Roberts, K. L., Shelton, H., Lycett, S. & Barclay, W. S. The short stalk length of highly pathogenic avian influenza H5N1 virus neuraminidase limits transmission of pandemic H1N1 virus in ferrets. *J. Virol.* **87**, 10539–10551 (2013).
17. Park, S. et al. Adaptive mutations of neuraminidase stalk truncation and deglycosylation confer enhanced pathogenicity of influenza A viruses. *Sci. Rep.* **7**, 10928 (2017).
18. Mänz, B. et al. Pandemic influenza A viruses escape from restriction by human MxA through adaptive mutations in the nucleoprotein. *PLoS Pathog.* **9**, e1003279 (2013).
19. Riegger, D. et al. The nucleoprotein of newly emerged H7N9 influenza A virus harbors a unique motif conferring resistance to antiviral human MxA. *J. Virol.* **89**, 2241–2252 (2015).
20. Shaw, A. E. et al. Fundamental properties of the mammalian innate immune system revealed by multispecies comparison of type I interferon responses. *PLoS Biol.* **15**, e2004086 (2017).
21. Kane, M. et al. Identification of interferon-stimulated genes with antiretroviral activity. *Cell Host Microbe.* **20**, 392–405 (2016).
22. Feeley, E. M. et al. IFITM3 inhibits influenza A virus infection by preventing cytosolic entry. *PLoS Pathog.* **7**, e1002337 (2011).
23. Verhelst, J., Parthoens, E., Schepens, B., Fiers, W. & Saelens, X. Interferon-inducible protein Mx1 inhibits influenza virus by interfering with functional viral ribonucleoprotein complex assembly. *J. Virol.* **86**, 13445–13455 (2012).
24. Wellington, D., Laurenson-Schafer, H., Abdel-Haq, A. & Dong, T. IFITM3: how genetics influence influenza infection demographically. *Biomed. J.* **42**, 19–26 (2019).
25. Rhodes, D. A., Stammers, M., Malcherek, G., Beck, S. & Trowsdale, J. The cluster of BTN genes in the extended major histocompatibility complex. *Genomics* **71**, 351–362 (2001).
26. Kumar, S., Stecher, G., Suleski, M. & Hedges, S. B. TimeTree: a resource for timelines, timetrees, and divergence times. *Mol. Biol. Evol.* **34**, 1812–1819 (2017).
27. Afrache, H., Pontarotti, P., Abi-Rached, L. & Olive, D. Evolutionary and polymorphism analyses reveal the central role of BTN3A2 in the concerted evolution of the BTN3 gene family. *Immunogenetics* **69**, 379–390 (2017).
28. Pinto, R. M., Lycett, S., Gaunt, E. & Digard, P. Accessory gene products of influenza A virus. *Cold Spring Harb. Perspect. Med.* https://doi.org/10.1101/cshperspect.a038380 (2021).
29. Naffakh, N., Tomoiu, A., Rameix-Welti, M. A. & van der Werf, S. Host restriction of avian influenza viruses at the level of the ribonucleoproteins. *Annu. Rev. Microbiol.* **62**, 403–424 (2008).
30. Patrono, L. V. et al. Archival influenza virus genomes from Europe reveal genomic variability during the 1918 pandemic. *Nat. Commun.* **13**, 2314 (2022).
31. van Lieshout, L. P. et al. A novel triple-mutant AAV6 capsid induces rapid and potent transgene expression in the muscle and respiratory tract of mice. *Mol. Ther. Methods Clin. Dev.* **9**, 323–329 (2018).
32. Portela, A. & Digard, P. The influenza virus nucleoprotein: a multifunctional RNA-binding protein pivotal to virus replication. *J. Gen. Virol.* **83**, 723–734 (2002).
33. Gabriel, G., Herwig, A. & Klenk, H. D. Interaction of polymerase subunit PB2 and NP with importin alpha1 is a determinant of host range of influenza A virus. *PLoS Pathog.* **4**, e11 (2008).
34. Hu, Y., Sneyd, H., Dekant, R. & Wang, J. Influenza A virus nucleoprotein: a highly conserved multi-functional viral protein as a hot antiviral drug target. *Curr. Top. Med. Chem.* **17**, 2271–2285 (2017).
35. Beaton, A. R. & Krug, R. M. Transcription antitermination during influenza viral template RNA synthesis requires the nucleocapsid protein and the absence of a 5′ capped end. *Proc. Natl Acad. Sci. USA* **83**, 6282–6286 (1986).
36. Chen, Y. et al. Rare variant MX1 alleles increase human susceptibility to zoonotic H7N9 influenza virus. *Science* **373**, 918–922 (2021).
37. Pu, J. et al. Evolution of the H9N2 influenza genotype that facilitated the genesis of the novel H7N9 virus. *Proc. Natl Acad. Sci. USA* **112**, 548–553 (2015).
38. He, J. et al. Genetic characterization of the first detected human case of avian influenza A (H5N6) in Anhui Province, East China. *Sci. Rep.* **8**, 15282 (2018).
39. de Jong, J. C., Claas, E. C., Osterhaus, A. D., Webster, R. G. & Lim, W. L. A pandemic warning? *Nature* **389**, 554 (1997).
40. Neumann, G., Chen, H., Gao, G. F., Shu, Y. & Kawaoka, Y. H5N1 influenza viruses: outbreaks and biological properties. *Cell Res.* **20**, 51–61 (2010).
41. Su, S. et al. Epidemiology, evolution, and pathogenesis of H7N9 influenza viruses in five epidemic waves since 2013 in China. *Trends Microbiol.* **25**, 713–728 (2017).
42. Harly, C. et al. Key implication of CD277/butyrophilin-3 (BTN3A) in cellular stress sensing by a major human γδ T-cell subset. *Blood* **120**, 2269–2279 (2012).
43. Arnett, H. A. & Viney, J. L. Immune modulation by butyrophilins. *Nat. Rev. Immunol.* **14**, 559–569 (2014).
44. Gu, S., Borowska, M. T., Boughter, C. T. & Adams, E. J. Butyrophilin3A proteins and Vγ9Vδ2 T cell activation. *Semin. Cell Dev. Biol.* **84**, 65–74 (2018).
45. Galão, R. P. et al. TRIM25 and ZAP target the Ebola virus ribonucleoprotein complex to mediate interferon-induced restriction. *PLoS Pathog.* **18**, e1010530 (2022).
46. Kuroda, M. et al. Identification of interferon-stimulated genes that attenuate Ebola virus infection. *Nat. Commun.* **11**, 2953 (2020).
47. Staeheli, P., Grob, R., Meier, E., Sutcliffe, J. G. & Haller, O. Influenza virus-susceptible mice carry Mx genes with a large deletion or a nonsense mutation. *Mol. Cell. Biol.* **8**, 4518–4523 (1988).
48. Guénet, J. L. & Bonhomme, F. Wild mice: an ever-increasing contribution to a popular mammalian model. *Trends Genet.* **19**, 24–31 (2003).
49. Zhang, B. et al. The nucleoprotein of influenza A virus inhibits the innate immune response by inducing mitophagy. *Autophagy* https://doi.org/10.1080/15548627.2022.2162798 (2023).
50. Philippon, D. A. M., Wu, P., Cowling, B. J. & Lau, E. H. Y. Avian influenza human infections at the human-animal interface. *J. Infect. Dis.* **222**, 528–537 (2020).
51. Adlhoch, C. et al. Avian influenza overview December 2021 - March 2022. *EFSA J.* **20**, e07289 (2022).
52. Agüero, M. et al. Highly pathogenic avian influenza A(H5N1) virus infection in farmed minks, Spain, October 2022. *Euro. Surveill.* https://doi.org/10.2807/1560-7917.Es.2023.28.3.2300001 (2023).
53. Bussey, K. A., Bousse, T. L., Desmet, E. A., Kim, B. & Takimoto, T. PB2 residue 271 plays a key role in enhanced polymerase activity of influenza A viruses in mammalian host cells. *J. Virol.* **84**, 4395–4406 (2010).
54. Burke, S. A. & Trock, S. C. Use of influenza risk assessment tool for prepandemic preparedness. *Emerg. Infect. Dis.* **24**, 471–477 (2018).

Methods

Cells, viruses and chemical treatments

MT4 (a gift from P. Bieniasz, Rockefeller University) suspension cells were cultured in Roswell Park Memorial Institute medium (Gibco) 1640 medium supplemented with 10% foetal bovine serum (FBS) (Gibco), 100 U ml^{-1} penicillin and 100 μg ml^{-1} streptomycin. MDCK cells (American Type Culture Collection, ATCC), human embryonic kidney cells (293T) (ATCC), human adenocarcinomic alveolar basal epithelial cells (A549) (ATCC) were cultured in Dulbecco's modified Eagle's medium (DMEM, Gibco) supplemented with 10% FBS (Gibco), 100 U ml^{-1} penicillin and 100 μg ml^{-1} streptomycin. MDCK cells expressing Sialyltransferase 1 (MDCK-SIAT, kindly provided by J. McCauley, The Francis Crick Institute) were further supplemented with 50 μg ml^{-1} geneticin. hTERT-immortalized primary human foetal lung fibroblasts were generated at the Centre for Virus Research and cultured in minimum essential medium supplemented with 10% FBS, 100 U ml^{-1} penicillin, 100 μg ml^{-1} streptomycin and 1× non-essential amino acids. Normal hBECs immortalized with CDK4 and hTERT (hBEC3-KT)[55] (UT Southwestern Medical Center) were kept in Keratinocyte serum-free medium (Gibco) supplemented with 50 μg ml^{-1} of bovine pituitary extract, 5 ng ml^{-1} of human recombinant epidermal growth factor, 100 U ml^{-1} penicillin and 100 μg ml^{-1} streptomycin. MT4 cells and A549 were authenticated using short tandem repeat analysis carried out by either the DNA Diagnostics Centre or Eurofins, and analysed using the DSMZ online short tandem repeat analysis tool.

Culture media of SCRPSY-modified cells was further supplemented with 1 μg ml^{-1} of puromycin dihydrochloride. All cell lines were regularly tested for mycoplasma contamination and passaged once or twice weekly.

A/Puerto Rico/8/1934 H1N1 (PR8), A/California/04/2009 H1N1 (Cal04), A/mallard/Netherlands/10-Cam/1999 H1N1 (Mallard), 6:2 reassortants of A/Anhui/1/2013 H7N9 (Anhui H7N9) containing PR8 segments 4 and 6 viruses, and other mutants and reassortants described in this study were generated by reverse genetics essentially as described previously[56]. Briefly, roughly 2×10^6 293T cells were transfected in Opti-MEM with pDUAL reverse genetics plasmids (250 ng of plasmid for each virus segment), using 4 μl of Lipofectamine 2000 according to the manufacturer's instructions. Twenty-four hours after transfection, the media was changed to serum-free DMEM supplemented with 0.14% bovine serum albumin (w/v) and 1 μg ml^{-1} of L-(tosylamido-2-phenyl) ethyl chloromethyl ketone (TPCK)-treated trypsin. Virus-containing supernatant was collected after a further 2-day incubation and propagated in MDCK cells. Clarified supernatant was collected when roughly 90% of cells demonstrated cytopathic effect (typically 36–72 hpi).

Other virus strains used in the study are the following: A/Udorn/307/1972 H3N2 (Udorn H3N2), A/Norway/3275 2018 H3N2 (Norway H3N2), A/Norway/3433/ 2018 H1N1 (Norway H1N1), A/ruddy shelduck/Mongolia/963V/2009 H3N8 (Ruddy shelduck H3N8), A/wild-duck/Italy/17VIR6926-1/2017 H5N2 (Wild duck H5N2), A/duck/Italy/18VIR4932-2/2018 H7N7 (Duck H7N7), A/turkey/Italy/16VIR8643-54/2016 H9N2 (Turkey H9N2). Udorn H3N2, Norway H1N1 and Ruddy shelduck H3N8 were propagated and plaqued in MDCK, whereas Norway H3N2 was grown and plaqued in MDCK-SIAT. Avian viruses wild duck H5N2, Duck H7N7 and Turkey H9N2 were propagated and plaqued in MDCK overexpressing *Gallus gallus* ANP32A.

CHX treatment consisted of incubation of cells with 100 μg ml^{-1} for 1 h before infection. Virus inoculum and media used throughout the experiment also contained the same concentration of CHX.

Arrayed ISG overexpression screening

Lentiviral transduction/flow cytometry-based screening was performed as previously described[57]. Briefly, MT4 cells were seeded in 96-well plates and further transduced with two SCRPSY-based lentiviral vector libraries consisting of 525 human and 345 macaque ISGs. At 48 h after transduction, cells were infected with PR8-GFP, Mallard-GFP or Cal04 7:1 PR8 segment 8 GFP (rescued as previously described[58]). After 10 h, cells were fixed and the percentage of transduced (TagRFP-positive) and IAV-infected (GFP-positive) cells was determined by flow cytometry using a Guava EasyCyte flow cytometer (Millipore).

The screens in Fig. 2e were performed in a similar manner. MT4, AA2, A549 naïve and overexpressing human ACE2 or 293T suspension cells were transduced with lentiviral ISG-expressing library as described above[59]. Forty-eight hours after transduction, cells were infected with reporter-expressing virus aiming to achieve a 10–50% infection. The panel of viruses used in Fig. 2e included: human mastadenovirus C (Adenovirus 5); Suid herpesvirus 1 (pseudorabies); human herpesvirus 1; bovine herpesvirus 1; Rift Valley fever phlebovirus; Dabie bandavius (severe fever with thrombocytopenia syndrome virus); Bunyamwera orthobunyavirus; bluetongue virus; Simian Rotavirus A/SA11; Chandipura vesiculovirus; Indiana vesiculovirus; Semliki Forest virus; Chikungunya virus; human immunodeficiency virus-1; IAV PR8, A/Puerto Rico/8/1934 (H1N1); IAV Cal04, A/California/04-061-MA/2009 (H1N1) rescued with PR8 segment 8; IAV Mallard, A/Mallard/Netherlands/10-Cam/1999 (H1N1); measles Ed-Zag vac; murine respirovirus (Sendai virus); mammalian orthorubulavirus 5 (parainfluenza virus 5 or simian virus 5); human metapneumovirus; human orthopneumovirus (human respiratory syncytial virus); bovine orthopneumovirus (bovine respiratory syncytial virus); human respirovirus 3 (parainfluenza virus 3) and Zika virus.

IAV infection

Monolayers of A549, MRC5T and hBEC3-KT cells were washed once with PBS and infected with virus diluted in serum-free medium for 1 h at 37 °C (multiplicity of infection (MOI) used is specified in the relevant figures). Medium was replaced with complete maintaining medium (for qPCR with reverse transcription (RT–qPCR) or western blot analysis) or serum-free medium supplemented with 0.14% BSA and 1 μg ml^{-1} TPCK-treated bovine pancreas trypsin (growth kinetics and quantification of infectious virus titres). Infectious titres were determined by plaque assay.

Virus quantification by plaque assay

Confluent monolayers of MDCK cells (1×10^6 or 2×10^6 cells seeded the day before infection in 12- or six-well plates, respectively) were washed once with PBS, infected with tenfold serial dilutions of virus and incubated for 1 h at 37 °C to allow virus adsorption to the cells. After virus removal, cells were overlaid with DMEM including 0.14% BSA, 1 μg ml^{-1} TPCK-treated trypsin and 1.2% Avicel and incubated for 3 days at 37 °C, 5% CO_2. After removing the overlay, cells were fixed with PBS:4% formaldehyde and stained with a 20% methanol:10% acetic acid:0.2% Coomassie Blue solution for at least 1 h. Staining solution was rinsed under tap water, plates were air-dried and plaques were then counted. Plaque assays for the avian viruses A/wild-duck/Italy/17VIR6926-1/2017 H5N2, A/duck/Italy/18VIR4932-2/2018 H7N7 and A/turkey/Italy/16VIR8643-54/2016 H9N2 were performed as described but using MDCK cells overexpressing galline ANP32A. Plaque assays for Cal04 backbone viruses were performed essentially as described but using MDCK-SIAT cells and a 3-day incubation period at 35 °C. Cells were then fixed, fixing solution was removed and cells were washed with PBS and permeabilized using PBS:0.2% (v/v) Triton X-100 for 10 min. After two PBS washes, cells were incubated with a mouse anti-NP antibody (diluted 1:1,000 in PBS:2% BSA) for 1 h on a rocking platform at room temperature. Following two PBS washes, cells were incubated with goat antimouse IgG-horseradish peroxidase (HRP) conjugated secondary antibody (diluted 1:1,000 in PBS:2% BSA) for 1 h in the same conditions. Cells were washed three times with PBS, TrueBlue peroxidase substrate was then added and cells were incubated at room temperature covered from direct light. When blue-stained plaques were visible, cells were

washed with water, allowed to dry and plaques were counted (under a stereo microscope, if required).

siRNA-mediated gene silencing

MCR5T (5×10^5 cells per well), hBEC3-KT (5×10^5 cells per well) or A549-based cells (3.5×10^5 cells per well) were seeded before transfection of siRNA molecules targeting BTN3A1, BTN3A3 or Mx1. Silencing of BTN3A1 and BTN3A3 was achieved using commercially available siRNAs: BTN3A1 siRNA1 (Thermo fisher Scientific assay ID s21922), BTN3A1 siRNA2 (Thermo fisher Scientific assay ID s21923), BTN3A1 siRNA3 (Qiagen material no. 1027415 catalogue no. SI00163772), BTN3A1 siRNA4 (Qiagen material no. 1027415 catalogue no. SI03021683), BTN3A3 siRNA1 (Thermo fisher Scientific assay ID s20305), BTN3A3 siRNA2 (Thermo fisher Scientific assay ID s20306), BTN3A3 siRNA3 (Qiagen material no. 1027415 catalogue no. SI00093660), BTN3A3 siRNA4 (Qiagen material no. 1027415 catalogue no. SI00093681). Negative controls were also purchased from the same two companies: Neg ctrl 1 (Thermo fisher Scientific catalogue no. AM4641), Neg ctrl 2 (Qiagen catalogue no. 1022076). Silencing of MX1 was accomplished using a commercially available pool of four different siRNAs (Dharmacon catalogue no. L-011735-00) with the respective negative control (Dharmacon catalogue no. D-001810-10). When transfecting, 20 pmol of siRNA was used with 3 µl of DharmaFECT 2 (Horizon Discovery) per well according to the manufacturer's protocol.

RNP reconstitution minireplicon reporter assay

Subconfluent monolayers of 293T-Empty and 293T-BTN3A3 cells (2×10^5 cells seeded in 24-well plates the previous day) were cotransfected in triplicate with 50 ng of each pcDNA3.1$^+$ plasmids encoding PB2, PB1, PA and NP along with 10 ng of transfection control plasmid (CMV-driven expression of Renilla luciferase) and 50 ng of a PolI-driven expression of vRNA or cRNA-like firefly luciferase reporter plasmids. As a negative control, transfections lacking the NP plasmid (empty pcDNA vector was used to balance plasmid intake) were also performed. Two days after transfection, medium was removed and cells were lysed with 120 µl of reporter lysis buffer. Cell debris was scraped off, lysates were collected into clean tubes and clarified by centrifugation (10,000 r.p.m. for 5 min at 4 °C) in a benchtop centrifuge. Luminescence was measured from 20 µl of lysate in opaque 96-well plates by using 25 µl of either luciferase assay reagent II or STOP & Glo (Dual-Luciferase reporter assay system) in an automatic injector and plate reader (injection speed 200 µl s^{-1}, gap 0.5 s and integration time 10 s).

In vitro translation assay

Total cellular RNA was isolated using from infected and CHX-treated cells using Qiagen RNeasy Kit according to the manufacturer's instructions. In vitro translation reactions were performed by using 3 µl of RNA in a TNT Coupled Reticulocyte Lysate system supplemented with 2 µCi of [^{35}S] cysteine and [^{35}S] methionine mix and incubated at 30 °C for 90 min. The reactions were denatured by mixing 1:1 in 4× Laemmli buffer and further heated for 5 min at 95 °C. Lysates were further analysed by SDS–PAGE followed by Coomassie staining and autoradiography of polyacrylamide gels. Gels were fixed with three 10-min incubations in a 50% methanol:10% acetic acid solution, transferred onto 3 mm Whatman filter paper, covered with cling film and dried in a gel dryer for 3 h at 80 °C for 2 h under vacuum. Dried gels were placed in a sealed cassette with an X-ray film for 48 h and films were developed using a Konica SRX-101A X-ograph film processor following the manufacturer's protocol.

RT–qPCR

Total RNA of CHX-treated and/or infected cells was extracted using the RNAdvance Blood kit (Beckman Coulter Life Sciences), including a DNase treatment, following the manufacturer's instructions. Extracted and DNase-treated RNA was used to perform strand-specific two-step RT–qPCR targeting the three different influenza RNA species, as previously described[60]. Briefly, a 5′ tagged primer is used for the cDNA synthesis, the reverse complement of which was then used as a forward primer in the real-time PCR step. Therefore, even in the event of primer-nonspecific complementary DNA (cDNA) synthesis, only the cDNA generated with the tagged primer will be detected and amplified in the real-time PCR. cDNA synthesis was performed with 5 µl of extracted RNA using the RevertAid kit (Thermo fisher) in a VeritiTM 96-well Thermal Cycler. qPCR reactions were performed with 2 µl of cDNA using the Brilliant III Ultra-Fast qPCR mastermix. qPCR was performed and analysed using the QuantStudio 3 thermocycler and software systems (Thermo Fisher Scientific). A list of primers and probes can be found in supplementary information. In vitro-synthesized T7-transcribed viral mRNA, vRNA and cRNA-like transcripts were diluted and used as a standard curve. Relative quantification of vRNA species was performed against GAPDH.

Cell fractionation

A549-Empty and A549-HsBTN3A3 cells were infected with PR8 and Mallard at an MOI of 3 for 45 min, 90 min or 6 h. Cells were then washed in ice-cold PBS and lysed with 50 mM Tris-HCl pH 7.5, 10 mM KCl, 5 mM $MgCl_2$, 0.5% NP40, 1 mM DTT, 10 mM sodium b-glycerophosphate and Halt Protease inhibitor (1×, EDTA-free) (Thermo Fisher 78429). Lysates were kept on ice for 10 min (gently vortexed every 2–3 min) and centrifuged at 1,000*g* for 5 min at 4 °C. The supernatant (cytoplasmic fraction) was transferred to a clean 1.5 ml tube and the nuclear fraction was washed thrice with the above-mentioned lysis buffer (centrifugations done for 5 min at 1,000*g*). The nuclear fraction was then incubated on ice for 30 min with 2× LDS (Thermo Fisher NP0007), 2× sample reducing agent (Thermo Fisher NP0004), Denarase (final concentration 25 U ml^{-1}) (c-LEcta 20804-100k) and 10 mM $MgCl_2$. The nuclear fraction was sonicated ten times for 20 s with 10-s intervals, before being centrifuged at 12,000*g* for 15 min. The supernatant was collected, and the pellet discarded. The cytoplasmic fraction was denatured using 1× LDS and 1× sample reducing agent.

In Fig. 4a, given the different times after infection and the different amounts of accumulated viral proteins between them, the three presented datasets originated from different volumes of lysate and different exposure times.

Immunoprecipitation

hBEC3-KT cells were infected with Mallard WT and Mallard F313Y at an MOI of 3 for 6 h and subsequently lysed[61]. Lysates were preclarified overnight at 4 °C with protein-A agarose beads (Sigma Aldrich P3476). Then 4 mg of protein lysates were incubated with 12 µg of either anti-NP or IgG control antibody overnight at 4 °C. Supernatants from the α-NP and IgG control were further incubated overnight at 4 °C with 12 µg of anti-BTN3A3 and IgG control antibody, respectively. Then 15 µl of Protein-A agarose beads were added for 1 h the next morning. Immunoprecipitations were then washed with 50 mM Tris-HCl, 500 mM sodium chloride and 0.5% Triton X-100 followed by 50 mM Tris-HCl only before being eluted using 2× LDS and 2× sample reducing agent. Immunoprecipitates were lysed and further subjected to immunoblotting targeting NP, PB2, PB1, PA and BTN3A3.

Immunoblotting

Total cell, immunoprecipitates or lysates from fractionation experiments were heated at 80 °C for 5 min and subjected to polyacrylamide gel electrophoresis using 3-(*N*-morpholino) propanesulfonic acid running buffer and transferred to polyvinylidene difluoride (Merck Millipore IPFL00010) membranes at 30 V for 90 min. Membranes were blocked for 1 h with 1× Tris-buffered saline with 0.2% Tween 20 (TBST)/5% milk, washed four times with 1× TBST and stained with primary antibodies diluted in 5% BSA BSA/0.01% sodium azide overnight

at 4 °C. After four 10-min 1× TBST washes, secondary antibodies were diluted in blocking buffer and incubated for 1 h at room temperature protected from direct light. Following four more washes in 1× TBST, membranes were imaged using the LI-COR CLx-Odyssey Imaging platform. Densitometry analysis was performed using the Image Studio Lite Software.

Immunofluorescence staining

The desired cell lines were seeded on 13 mm round glass coverslips in 24-well dishes. After infection and/or transfection, cells were washed twice with PBS and fixed with 4% formaldehyde in PBS for 20 min followed by three PBS washes. Cells were permeabilized with PBS:1% Triton X-100 for 10 min at room temperature. Following three washes with PBS, cells were blocked with 1 ml of PBS:1% BSA for 1 h followed by incubation for 1 h with 200 µl of primary antibodies at the appropriate dilutions (for the detection of BTN3A3 in hBEC3-KT cells, the primary antibody was incubated overnight at 4 °C). Three 1 ml PBS:0.2% Tween20 washes were then executed to remove unbound antisera followed by incubation of secondary antibodies in the same volume. 4′,6-Diamidino-2-phenylindole (DAPI) (100 ng ml^{-1}) was diluted in blocking buffer and incubated for 10 min. When using HCS CellMask Deep Red Stain (2 µg ml^{-1}, Thermo Fisher Scientific), this was added after DAPI staining for 30 min followed by three PBS washes. After the labelling steps were completed, coverslips were washed three more times with water and mounted upside down on glass slides with AF1 Mounting media (CitiFluor). Coverslips were imaged using the ZEISS LSM 710 or LSM 880 (with Airyscan) confocal laser scanning microscopes. Quantification of nuclear and cytoplasmic proteins from confocal images was performed using a pipeline created on CellProfilerTM. Pipeline details are provided in the Supplementary Information.

Immunohistochemistry

We analysed sections (3 µm thick) of formalin-fixed and paraffin-embedded healthy human lung (n = 2) and respiratory nasal epithelium tissues (n = 5). Health tissues were purchased from Amsbio and were obtained from five female and one male donors ranging in age between 31 and 62 years old of Caucasian and Asian ethnicity (one of them of unknown ethnicity). Tissues were stained with a rabbit anti-BTN3A3 antibody (HPA 007904, Atlas antibodies) for 90 min at room temperature after pressure cooking in sodium citrate. For visualization, EnVision Detection System HRP, peroxidase/DAB (rabbit, K500711, Agilent) was used according to the manufacturer's instructions. The specificity of the antibody was validated on formalin-fixed and paraffin-embedded A549-Empty and A549-HsBTN3A3 cell pellets. Negative control sections included an isotype control on a consecutive serial section. Slides were scanned with a Leica Aperio Versa 8 slide scanner (Leica Biosystems) and images were acquired with a Aperio ImageScope software (Leica Biosystems).

Mouse lung tissues were stained with a rabbit anti-BTN3A3 antibody (HPA 007904, Atlas antibodies) and anti-GFP antibody (Cell Signalling 2555S) for 90 min at room temperature after pressure cooking in sodium citrate. For visualization, EnVision Detection System HRP, peroxidase/DAB (rabbit, Agilent K500711) was used according to the manufacturer's instructions.

AAV vectors

AAV vector genome plasmids were engineered to encode a ubiquitous CASI promoter[62] driving expression of the human BTN3A3 gene (or GFP, as a negative control) followed by a woodchuck hepatitis virus post-transcriptional regulatory element[62] and a SV40 polyA signal all contained between AAV2 inverted terminal repeats. AAV vectors were produced by cotransfection of human embryonic kidney 293 cells with genome and packaging plasmids as described previously[62]. Vectors pseudotyped with AAV6.2FF were purified by use of a heparin column[62]. AAV vector titres were determined by qPCR analysis as described elsewhere[63].

Mouse infections

Six-week old female C57BL/6 mice were purchased from Envigo. Animals were maintained at the University of Glasgow under specific pathogen free conditions in accordance with UK home office regulations (Project Licence PP1902420) and approved by the University of Glasgow ethics committee. Following 7 days of acclimatization, the mice were briefly anaesthetized using inhaled isoflurane and transduced with 1×10^{11} virus genomes of AAV. Mice received either AAV-GFP or AAV-BTN3A3 in 50 µl of PBS intranasally. Twenty-one days after AAV instillation, mice were infected with Cal04 and Cal04 V313F (both 6:2 with PR8 haemagglutinin and neuraminidase). Group sizes were chosen on the bases of a pilot experiment to assess AAV transduction and previous experience[64]. No specific randomization were conducted. Analysis of data was conducted in an unbiased manner but no specific blinding was used for the researchers carrying out virus titration from mice tissues. Mice were briefly anaesthetized using inhaled isoflurane and intranasally infected with 5×10^3 PFU of each virus in 20 µl of PBS. A total of four infected mice showed technically poor infections with bubbles forming from the nostrils and therefore were discarded from the experiment. All mice were euthanized by cervical dislocation 3 days post infection. Weight loss for all groups did not exceed the humane cut-off point of 20%. Once euthanized, mouse lungs were extracted and frozen at −80 °C. Lungs were thawed, weighed and homogenized with 1 ml of DMEM. Homogenates were cleared by centrifugation (3,000 r.p.m., 4 °C) and titrated by plaque assay.

In silico identification of BTN3 homologues

To identify proteins expressed by other species, homologous to the human BTN3 genes, we performed a Blastp search (v.2.8.1) against all available members of the Haplorrhini suborder in the National Center for Biotechnology Information (NCBI) blast protein refseq database v.5 (cut-off 1×10^{-6}, as of 6 April 2021)[65]. The human BTN3A3 protein sequence (NP_008925.1) was used as a probe for the BLAST search. The isoform with the longest sequence was kept for each protein product annotated with the same name. Similarly, Blastp with human BTN3A3 was used for identifying proteins expressed by non-primate species susceptible to IAV infection: *Gallus*, *Anas platyrhynchos*, *Equus caballus* and *Sus scrofa* and more distant human paralogues (Extended Data Fig. 2 and Supplementary Table 5).

Protein members of the butyrophilin 3 subfamily retrieved from the BLAST search were manually cross-checked with proteins in the Ensembl database[66] and if the protein sequences were not identical between the two databases the sequence with highest similarity to the human BTN3A3 protein sequence was retained. A total of 30 proteins were retrieved from the following species: Pan troglodytes, *Cebus imitator*, *Equus caballus*, *Homo sapiens*, *Gorilla gorilla gorilla*, *Chlorocebus sabaeus*, *Macaca mulatta*, *Pongo abelii*, *Carlito syrichta*, *Mandrillus leucophaeus*, *Callithrix jacchus*, *Nomascus leucogenys* and *Rhinopithecus roxellana*.

A custom set of Pfam hmm profiles were used for identifying the conserved domains in the proteins, comprising the immunoglobulin V-set domain (PF07686), CD80-like C2-set immunoglobulin domain (PF08205), PRY (PF13765) and SPRY (PF00622) domains. All protein sequences were scanned with the profile set using hmmscan (HMMER v.3.3)[67]. The best hit for each identified domain was extracted from the protein sequence aligned with the respective domain segments using mafft (v7.453, --maxiterate 1000 --localpair)[68]. Protein alignments were converted to codon alignments using pal2nal[69]. Phylogenies for each separate domain alignment (Extended Data Fig. 4) and concatenated domain sequences (Extended Data Fig. 2) were reconstructed using iqtree (v.1.6.12)[70] with the best suited substitution model selected by the iqtree '-m TEST' option and 10,000 ultrafast bootstrap replicates.

IAV phylogenetic analysis

A total of 35,477 full-length NP-coding sequences unique on the nucleotide level (identical sequences collapsed) were retrieved from the NCBI Flu database (https://www.ncbi.nlm.nih.gov/genomes/FLU/Database/nph-select.cgi?go=database), as of 8 June 2021, sampled until the end of 2020), only including type A influenza sequences annotated to have been isolated from avian, canine, equine, human and swine hosts. Sequences with ambiguous nucleotides and internal stop codons were removed, resulting in a dataset of 34,079 sequences. The corresponding protein sequences were aligned using mafft (v7.453, --maxiterate 1000 --localpair)[68] and then converted to a codon alignment with pal2nal (ref. 69). Metadata associated with each sequence accession were retrieved and tabulated. Numbering of NP amino acid residues was assigned on the basis of the PR8 sequence. Therefore, the six-amino-acid N-terminal extension of 2009 pH1N1 viruses were not considered for the residue numbering (that is, amino acid residue M6 was considered M1).

To reduce oversampling of related sequences the dataset was clustered with a minimum sequence identity of 0.99 using MMseqs2 (--min-seq-id 0.99 --cov-mode 0)[71]. One representative was kept from each cluster leading to a filtered dataset of 14,665 sequences. The codon alignment of the filtered set was used to reconstruct a phylogeny with iqtree under a GTR+I+G4 model (selected as the most appropriate model with the '-m TEST' option)[70]. The resulting phylogeny was then time-calibrated using TreeTime[72] (Fig. 3c). Eleven sequences with annotated dates inconsistent with the root-to-tip regression were subsequently excluded from the analysis.

To explore the H7N9 epidemic NP clade in more detail, representative sequences from this broader avian NP clade (Fig. 5c), as well as the unfiltered sequences from each representative's corresponding cluster, were retrieved (3,150 sequences). The codon alignment of these NP sequences was used to infer a more detailed maximum likelihood phylogenetic reconstruction of this particular clade (iqtree under a GTR+I+F+G4 model with 10,000 ultrafast bootstrap replicates)[70] and time-calibrated using TreeTime as described above[72] (Fig. 5c). All phylogenies were visualized using the ggtree R package[73], unless stated otherwise. Tree statistics were analysed using the ete3 Python package[74].

GISAID sequence analysis

Protein sequences from atypical, avian-only serotypes (H1–H18) were retrieved from the GISAID database (http://gisaid.org/) for avian and human hosts (Supplementary Tables 2 and 4). Isolates were filtered for having all eight segments and having been sampled until 1 January 2023. The NP, haemagglutinin and PB2 proteins were downloaded for each isolate and aligned using mafft (v7.453, --maxiterate 1000 --localpair)[68]. NP and PB2 residues at sites of interest and haemagglutinin polybasic cleavage site presence (identified as having three or more K/R residues at the corresponding region) were summarized along with sequence metadata using Python3. GISAID acknowledgements for all analysed sequences are provided in Supplementary Tables 7 and 8.

Biosafety considerations

All experiments were performed in accordance with national regulations. Work was approved by the local GM Safety Committee (University of Glasgow GM Centre 223) and licensing authorities of the United Kingdom (Health & Safety Executive). To investigate the determinants of BTN3A3 resistance, mutations were introduced into the low-pathogenicity avian strain H1N1 Mallard (A/mallard/Netherlands/10-Cam/1999, H1N1), the human strain Cal04, PR8 or a (6+2) reassortant of an avian H7N9 strain with PR8. The H7N9/PR8 reassortant contained the 'internal' genes from H7N9 and the 'external' (glycoprotein) genes from PR8. PR8 is a human IAV strain that is greatly attenuated due to extensive laboratory passage in the mouse[75,76]. In terms of biosafety, two classes of mutation were designed. The first class of mutation aimed to convert a BTN3A3-sensitive phenotype into a resistant one. This was only carried out for the low-pathogenicity avian H1N1 Mallard strain. As noted before in the text, many circulating avian lineages already possess a BTN3A3-resistant genotype and therefore none of the mutants we generated pose a greater biosafety risk than viruses already in circulation. The second class of mutation aimed to convert a BTN3A3 insensitive phenotype into a sensitive one. These mutations, which were carried out with PR8, Cal04 and H7N9/PR8 strains, would be expected to attenuate viral growth in humans still further and would therefore reduce biosafety risks.

Experiments with IAVs described above were carried out at Biosafety Level 2. Most of the fluorescent viruses used in Fig. 2e were also used in Biosafety Level 2. Experiments performed with Severe fever with thrombocytopenia syndrome virus, Chikungunya virus, SARS-CoV-2, Bluetongue virus-8 and Human immunodeficiency virus-1 were conducted at Biosafety Level 3.

Reproducibility

Original source images for data obtained by electrophoresis, shown as cropped images in the figures in this study, are presented in Supplementary Fig. 1. Images shown throughout the paper are representative images of experiments as follows. Western blotting in Fig. 1c shows similar levels of BTN3A3 knockdown using four distinct guides in two different cell lines. Figure 1c shows one of three independent experiments, which were then analysed in Fig. 1d. The micrographs in Fig. 1e show a field of tissue sections collected from healthy nasal or lung tissues from one donor and probed with BTN3A3 or isotype control antibodies. Images are representative of several other fields of the same section. Similar images were obtained in the same experiment from four other donors for the respiratory nasal epithelium and one more donor for the lungs. Results obtained in the lungs were further validated by the transcriptomic data shown in Extended Data Fig. 1c,d. Western blotting in Fig. 2a was carried out to show overexpression of the respective BTN3 proteins, and it shows the specificity of antibodies against such proteins. These and other anti-BTN3 antibodies were then used for several experiments (Figs. 3e and 4a,c and Extended Data Figs. 1a,e, 3, 8 and 9). Image of western blotting in Fig. 2c is representative of two independent experiments. Images in Fig. 3e are western blots carried out once to validate the expression of Mx1 and BTN3A3 in stable cells then used for experiments shown in Fig. 3f. Micrographs in Fig. 3g are representative images of lung sections from single mock-, AAV-GFP- and AAV-BTN3A3-transduced mouse lungs. Similar images were obtained in nine more mice (a total of three mice per condition). Images from western blots in Fig. 4a,d are representative of three independent experiments. Western blot images in Fig. 4c were performed once and represent expression controls of one of the three experiments shown in Fig. 4b. Micrographs in Fig. 4e are representative images of four independent experiments (further analysed in Fig. 4i–j). Western blotting in Extended Data Fig. 1a shows similar levels of BTN3A1 knockdown using four distinct guides in two different cell lines. Extended Data Fig. 1 shows one of three independent experiments that were analysed in Extended Data Fig. 1b. Western blots in Extended Data Fig. 1e represents an experiment showing expression of BTN3A3, RSAD2 and pSTAT1 following IFN treatments in four different cell lines. Western blotting in Extended Data Fig. 3b was performed from one of the two independent experiments carried out in Extended Data Fig. 3a. Image of western blotting in Extended Data Fig. 7a shows the siRNA-driven Mx1 knockdown of one of the three experiments carried out in Extended Data Fig. 7b. Western blotting in Extended Data Fig. 8b was performed from one of the three independent experiments carried out in Extended Data Fig. 8a and validates the expression of RNP proteins. Extended Data Fig. 9a–c are representative images of western blotting of three independent experiments. The micrograph in Extended Data Fig. 10a is a representative image of four independent experiments (further analysed in Extended Data Fig. 10b,c).

Reporting summary

Further information on research design is available in the Nature Portfolio Reporting Summary linked to this article.

Data availability

Alignments and raw phylogenetic data related to this study can be found in the following GitHub repository: https://github.com/spyros-lytras/BTN3A3_IAV. Source data related to the animal experiments illustrated in Fig. 3h are available in Supplementary Table 9. Gel source data are available in Supplementary Fig. 1.

55. Ramirez, R. D. et al. Immortalization of human bronchial epithelial cells in the absence of viral oncoproteins. *Cancer Res.* **64**, 9027–9034 (2004).
56. Wit, E. D. et al. Efficient generation and growth of influenza virus A/PR/8/34 from eight cDNA fragments. *Virus Res.* **103**, 155–161 (2004).
57. Schoggins, J. W. et al. A diverse range of gene products are effectors of the type I interferon antiviral response. *Nature* **472**, 481–485 (2011).
58. Rihn, S. J. et al. TRIM69 inhibits vesicular stomatitis Indiana virus. *J. Virol.* https://doi.org/10.1128/JVI.00951-19 (2019).
59. Rihn, S. J. et al. A plasmid DNA-launched SARS-CoV-2 reverse genetics system and coronavirus toolkit for COVID-19 research. *PLoS Biol.* **19**, e3001091 (2021).
60. Kawakami, E. et al. Strand-specific real-time RT-PCR for distinguishing influenza vRNA, cRNA, and mRNA. *J. Virol. Methods* **173**, 1–6 (2011).
61. Bakshi, S., Taylor, J., Strickson, S., McCartney, T. & Cohen, P. Identification of TBK1 complexes required for the phosphorylation of IRF3 and the production of interferon β. *Biochem. J.* **474**, 1163–1174 (2017).
62. Zufferey, R., Donello, J. E., Trono, D. & Hope, T. J. Woodchuck hepatitis virus posttranscriptional regulatory element enhances expression of transgenes delivered by retroviral vectors. *J. Virol.* **73**, 2886–2892 (1999).
63. Rghei, A. D. et al. Production of adeno-associated virus vectors in cell stacks for preclinical studies in large animal models. *J. Vis. Exp.* https://doi.org/10.3791/62727 (2021).
64. MacLeod, M. K. et al. Vaccine adjuvants aluminum and monophosphoryl lipid A provide distinct signals to generate protective cytotoxic memory CD8 T cells. *Proc. Natl Acad. Sci. USA* **108**, 7914–7919 (2011).
65. Camacho, C. et al. BLAST+: architecture and applications. *BMC Bioinf.* **10**, 421 (2009).
66. Cunningham, F. et al. Ensembl 2022. *Nucleic Acids Res.* **50**, D988–d995 (2022).
67. Mistry, J., Finn, R. D., Eddy, S. R., Bateman, A. & Punta, M. Challenges in homology search: HMMER3 and convergent evolution of coiled-coil regions. *Nucleic Acids Res.* **41**, e121 (2013).
68. Katoh, K. & Standley, D. M. MAFFT multiple sequence alignment software version 7: improvements in performance and usability. *Mol. Biol. Evol.* **30**, 772–780 (2013).
69. Suyama, M., Torrents, D. & Bork, P. PAL2NAL: robust conversion of protein sequence alignments into the corresponding codon alignments. *Nucleic Acids Res.* **34**, W609–W612 (2006).
70. Nguyen, L. T., Schmidt, H. A., von Haeseler, A. & Minh, B. Q. IQ-TREE: a fast and effective stochastic algorithm for estimating maximum-likelihood phylogenies. *Mol. Biol. Evol.* **32**, 268–274 (2015).
71. Steinegger, M. & Söding, J. MMseqs2 enables sensitive protein sequence searching for the analysis of massive data sets. *Nat. Biotechnol.* **35**, 1026–1028 (2017).
72. Sagulenko, P., Puller, V. & Neher, R. A. TreeTime: maximum-likelihood phylodynamic analysis. *Virus Evol.* **4**, vex042 (2018).
73. Yu, G. Using ggtree to visualize data on tree-like structures. *Curr. Protoc. Bioinformatics* **69**, e96 (2020).
74. Huerta-Cepas, J., Serra, F. & Bork, P. ETE 3: reconstruction, analysis, and visualization of phylogenomic data. *Mol. Biol. Evol.* **33**, 1635–1638 (2016).
75. Beare, A. S. & Hall, T. S. Recombinant influenza-A viruses as live vaccines for man. Report to the Medical Research Council's Committee on Influenza and other Respiratory Virus Vaccines. *Lancet* **2**, 1271–1273 (1971).
76. Beare, A. S., Schild, G. C. & Craig, J. W. Trials in man with live recombinants made from A/PR/8/34 (H0 N1) and wild H3 N2 influenza viruses. *Lancet* **2**, 729–732 (1975).

Acknowledgements We are thankful to the authors, originating and submitting laboratories of the sequences from GISAID's EpiFlu Database on which some of this research is based (Supplementary Tables 7 and 8). We thank P. Murcia (MRC-University of Glasgow Centre for Virus Research) for providing clinical virus isolates and fruitful discussions, and M. Peiris (The University of Hong Kong) who kindly provided A/ruddy shelduck/Mongolia/963V/2009 (H3N8). We are grateful to S. Bhat, M. Iqbal (The Pirbright Institute), L. Tiley, R. Fouchier (Erasmus MC) and D. Perez (The University of Georgia) for providing the reverse genetics systems of the A/Anhui/1/2013 (H7N9) and A/mallard/Netherlands/10-Cam/1999 (H1N1), A/Puerto Rico/8/1934 (H1N1) and A/California/04-061-MA/2009 (H1N1) viruses, respectively. We acknowledge J. Mccauley (The Crick Institute) for sharing the MDCK-SIAT cells. This work was supported by the UK Medical Research Council (grant no. MC_UU_12016/10) awarded to M.P. and S.J.W. and the following grants: Wellcome Trust grant no. 206369/Z/17/Z (to M.P.); Biotechnology and Biological Sciences Research Council (BBSRC) grant no. BB/P013740/1 awarded to F.G. and P.D.; grant no. BBSRC BB/S00114X/1 awarded to F.G., P.D. and S.J.W.; EU Horizon2020: DELTA-FLU (grant no. 727922) awarded to P.D. and I.M.; Natural Sciences and Engineering Research Council of Canada Discovery grant (no. RGPIN-2018-04737) awarded to S.K.W.; Daphne Jackson Fellowship funded by Medical Research Scotland awarded to S.S.; MRC Career Development Award and Transition Support Award (grant nos. MR/N008618/1 and MR/V035789/1) to E.H.; Wellcome Trust grant no. 210703/Z/18/Z awarded to M.K.L.M. and Medical Research Council grant no. MC_UU_12014/5 awarded to C.B., Q.G. and J.H. are funded by Medical Research Council grant no. MC_UU_12014/12.

Author contributions Conceptualization was done by R.M.P., S.J.W. and M.P. The methodology was developed by R.M.P., S.B., S.L., M.K.Z., S.S., J.C.W., V.H., K.E.H., L.O., S.K.W. and M.K.L.M. Software was provided by S.L., J.H. and Q.G. Validation was done by R.M.P., S.B., S.L., M.K.Z., J.C.W., V.H. and K.E.H. Formal analysis was carried out by R.M.P., S.B., S.L., M.K.Z., S.S., V.H., M. Varjak, N.C.-R., M.C.R., M. Varela and J.H. The investigation was carried out by R.M.P., S.B., S.L., M.K.Z., S.S., J.C.W., V.H., M. Varjak, N.C.-R., M.C.R., M. Varela, L.O., A.W., C.L., Y.P., E.V., M.L.T., W.F., K.E.H., A.T., O.D. and C.D. Resources were provided by R.M.P., A.T., C.B., E.H., P.D., I.M., S.K.W., S.J.W. and M.P. Data were curated by R.M.P., S.L., M. Varjak, N.C.-R., M.C.R., M. Varela, A.W. and E.V. The original draft preparation and writing were done by R.M.P., S.B., S.L., M.K.Z., J.C.W., V.H., M.L.T., S.K.W. and M.P. Review and editing of the draft were done by R.M.P., S.B., S.L., M.K.Z., S.S., J.C.W., V.H., M.V.k., N.C.-R., M.C.R., M. Varela, A.W., C.L., J.H., E.V., M.L.T., W.F., K.E.H., Q.G., L.O., A.T., O.D., F.G., E.H., P.D., I.M., S.K.W., M.K.L.M., S.J.W. and M.P. Visualization was done by R.M.P., S.B., S.L. and M.P. Supervision was done by R.M.P., J.H., C.B., S.K.W., M.K.L.M., S.J.W. and M.P. Project administration was done by S.J.W. and M.P. Funding was acquired by S.S., C.B., F.G., P.D., I.M., S.K.W., M.K.L.M., S.J.W. and M.P.

Competing interests P.D. is a member of the Science Advisory Council's Exotic and Emerging Animal Diseases subgroup (SAC-ED) for the UK Government's Department for Environment, Food & Rural Affairs (Defra) and was part of SAC-ED's independent expert Scientific Advisory Group in highly pathogenic avian influenza. S.K.W. is an inventor on issued patents in Canada and the United States for the AAV6.2FF capsid, which are owned by the University of Guelph, and licensed to Avamab Pharma Inc., Inspire Biotherapeutics, and Cellastra Inc. M.P. is a member of the Standing Committee on Pandemic Preparedness of the Scottish Government. The remaining authors declare no competing interests.

Additional information

Supplementary information The online version contains supplementary material available at https://doi.org/10.1038/s41586-023-06261-8.

Correspondence and requests for materials should be addressed to Massimo Palmarini.

Peer review information *Nature* thanks Andrew Mehle, Peter Staeheli, Michael Worobey and the other, anonymous, reviewer(s) for their contribution to the peer review of this work. Peer reviewer reports are available.

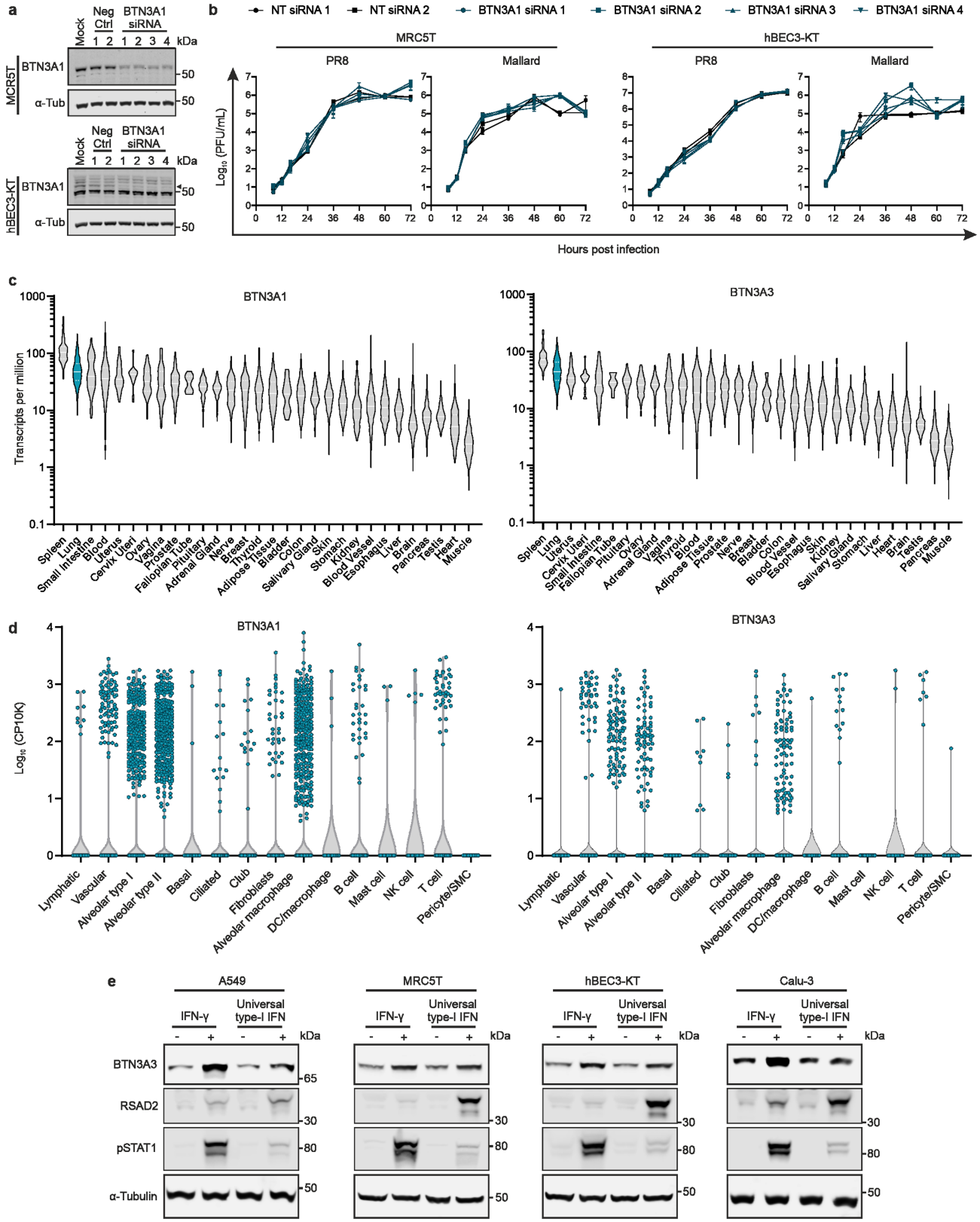

Extended Data Fig. 1 | See next page for caption.

Extended Data Fig. 1 | Activity and expression of BTN3A1 and BTN3A3 in cell lines and human tissues. a, siRNA knock-down of BTN3A1 in MRC5T and hBEC3-KT. Cells were transfected with scrambled (Neg ctrl) or BTN3A1-targeting siRNAs, and protein levels in the resulting cell lysates were assessed by western blotting. α-Tubulin was used as loading control. Arrows indicate the band corresponding to BTN3A1. For gel source data, see Supplementary Fig. 1. **b**, Graphs showing the replication kinetics of PR8 and Mallard in siRNA-treated MRC5T and hBEC3-KT cells. Cells were infected with a MOI of 0.001, supernatants were collected at the indicated times post infection and viruses titrated by plaque assay. Data are mean +/− SEM of 3 independent experiments (each using 2 technical replicates). Statistical significance between groups was measured by a 2-way ANOVA. Comparisons were made between area under the curve of the different BTN3A1 siRNA treatment conditions and the average of the two negative controls. No statistically significant differences were found. **c**, Organ-dependent bulk tissue gene expression. Lung samples are highlighted in blue. **d**, Lung single cell tissue expression. Data in **c** and **d** were obtained from the GTEx Portal (www.gtexportal.org). **e**, Western blotting of cell lysates obtained from A549, MRC5T, hBEC3-KT and Calu-3 treated with either IFN-γ or universal type-I IFN. Treatment with IFN was for 16h in A549, MRC5T, hBEC3-KT and for 24h in Calu-3 cells. pSTAT1 and RSAD2/Viperin were used as IFN induction controls and α-Tubulin as loading control. For gel source data, see Supplementary Fig. 1.

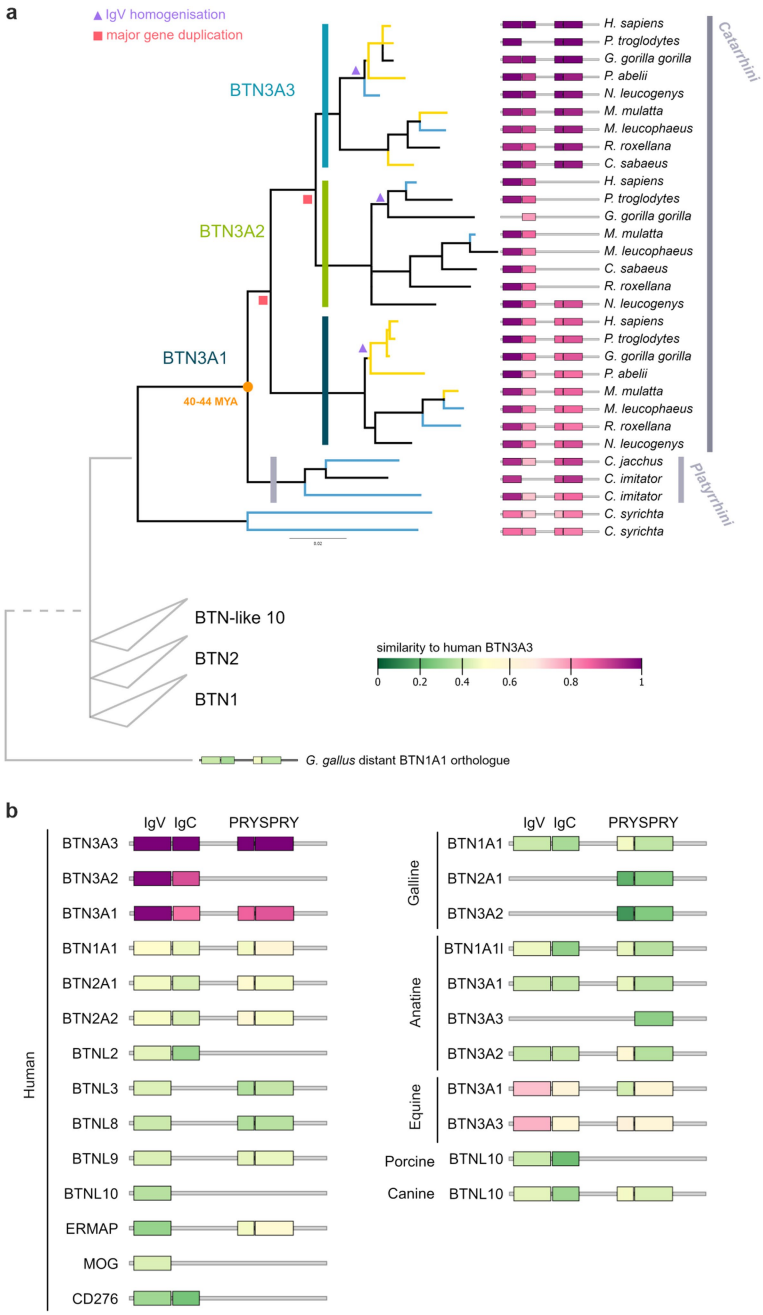

Extended Data Fig. 2 | Evolution of BTNs. a, Maximum likelihood phylogeny of concatenated protein domain coding sequences of the *Haplorrhini* BTN3 genes (K2P+G4 substitution model). Nodes with bootstrap support below 60 have been collapsed. Branches confirmed to have or not have anti-avian IAV activity (described in b) are highlighted in yellow and blue, respectively. Branches not tested were kept black. Relation to more distant tested homologues and orthologous/paralogous gene families are shown as a schematic in grey. IgV homogenization events, major gene duplications and gene subfamilies are annotated on the phylogeny. Presence of each of the four protein domains (IgV, IgC, PRY and SPRY) is annotated on the right of each tree tip and coloured by pairwise amino acid similarity to the respective domain of the human BTN3A3. Species names and taxonomic classification is annotated on the right. The median divergence time between *Catarrhini* and *Platyrrhini* was retrieved from TimeTree (http://timetree.org/). **b**, Schematic representation of domain organisation and sequence similarity of the indicated proteins.

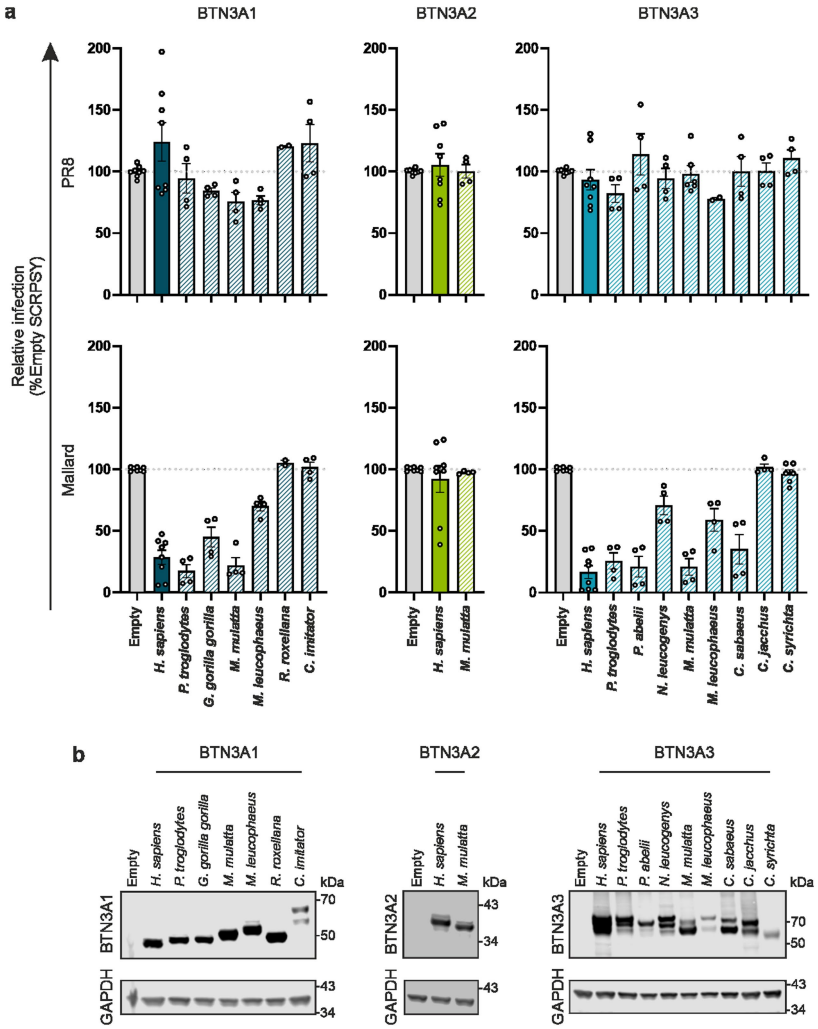

Extended Data Fig. 3 | Evolution of antiviral activity of BTNs. a, A549 cells were transiently transduced with SCRPSY lentiviruses expressing the indicated BTN proteins and challenged with PR8- or Mallard-GFP. Eight hours post infection, the percentage of GFP-positive cells was measured by flow cytometry. Data are mean +/− SEM of 2 independent experiments which both gave similar results. **b**, Western blotting of cell lysates obtained from A549 cells transiently transduced with SCPRSY lentiviruses expressing different BTN proteins. GAPDH was used as loading control. For gel source data, see Supplementary Fig. 1.

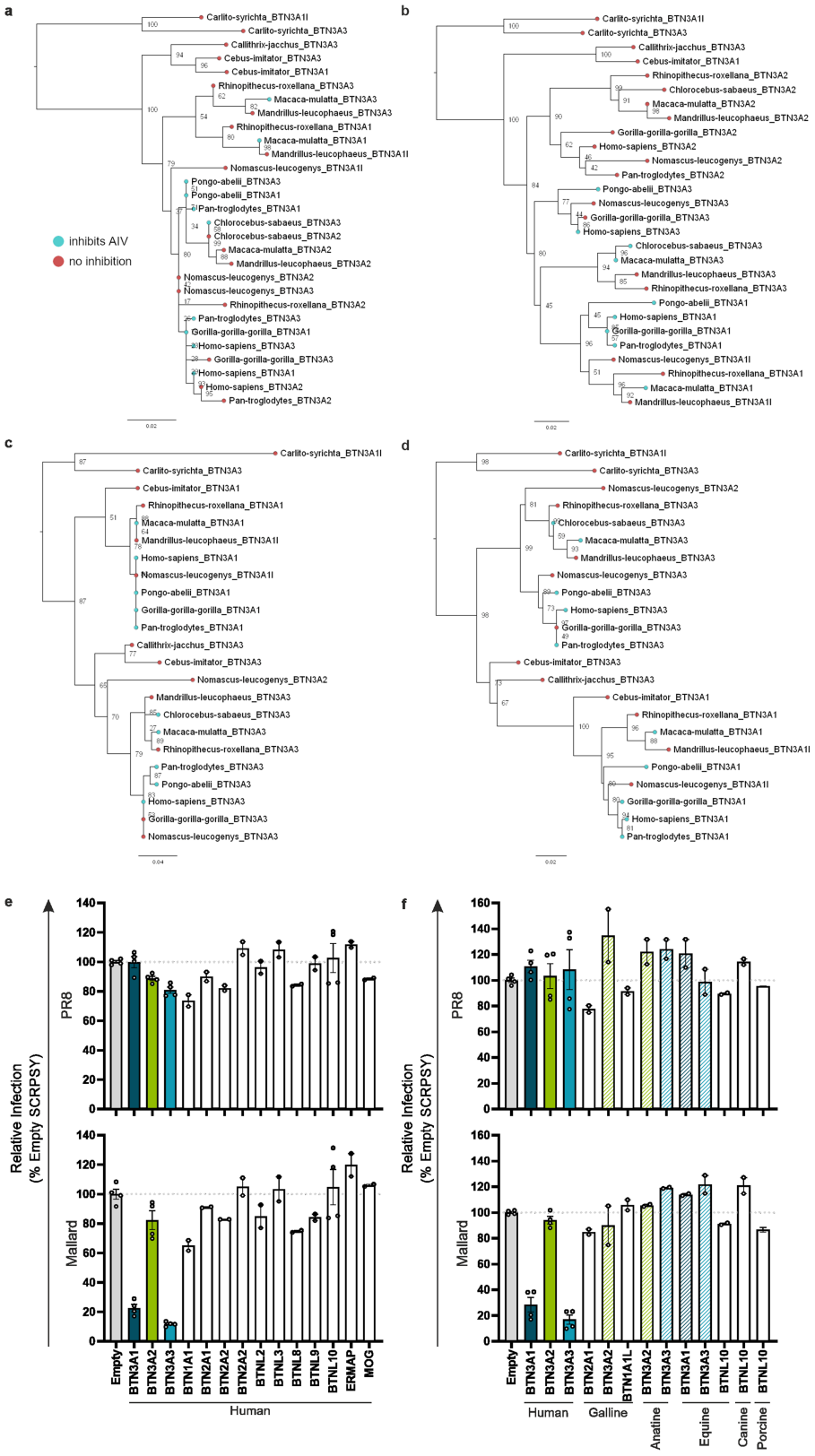

Extended Data Fig. 4 | See next page for caption.

Extended Data Fig. 4 | Phylogeny of BTN3 domains and antiviral activity of BTN orthologues and paralogues. a-d, maximum likelihood *Haplorrhini* BTN3 gene coding sequence phylogenies of separate domains: IgV (**a**), IgC (**b**), PRY (**c**), SPRY (**d**) under a K2P+G4 substitution model. Trees are rooted at the *C. syrichta* branch and node confidence values (10,000 bootstrap replicates) are annotated on each node. Tip shapes are coloured by whether each gene exhibits anti-AIV activity (consistent with Fig. 3a). Phylogenies were visualised using FigTree. **e**–**f**, A549 cells were transiently transduced with SCRPSY lentiviruses expressing the indicated BTN proteins and challenged with PR8- or Mallard-GFP. Eight hours post-infection, percentage of RFP-positive cells and its subpopulation of GFP-positive cells was measured by flow cytometry. Data are mean +/− SEM of 2 independent experiments which both gave similar results. Detection of these proteins was not possible using commercially available antibodies, due to their genetic divergence compared to human BTN3A1-3. Therefore, tagging of these BTN genes was attempted by introducing a C-terminal FLAG. Despite their protein expression being successfully detected using an anti-FLAG antibody, the addition of FLAG to human BTN3A3 and other BTN genes resulted in the abolishment of their antiviral activity. Cloning of the genes indicated above was conducted in the same way as those constructs shown in Extended Data Fig. 3.

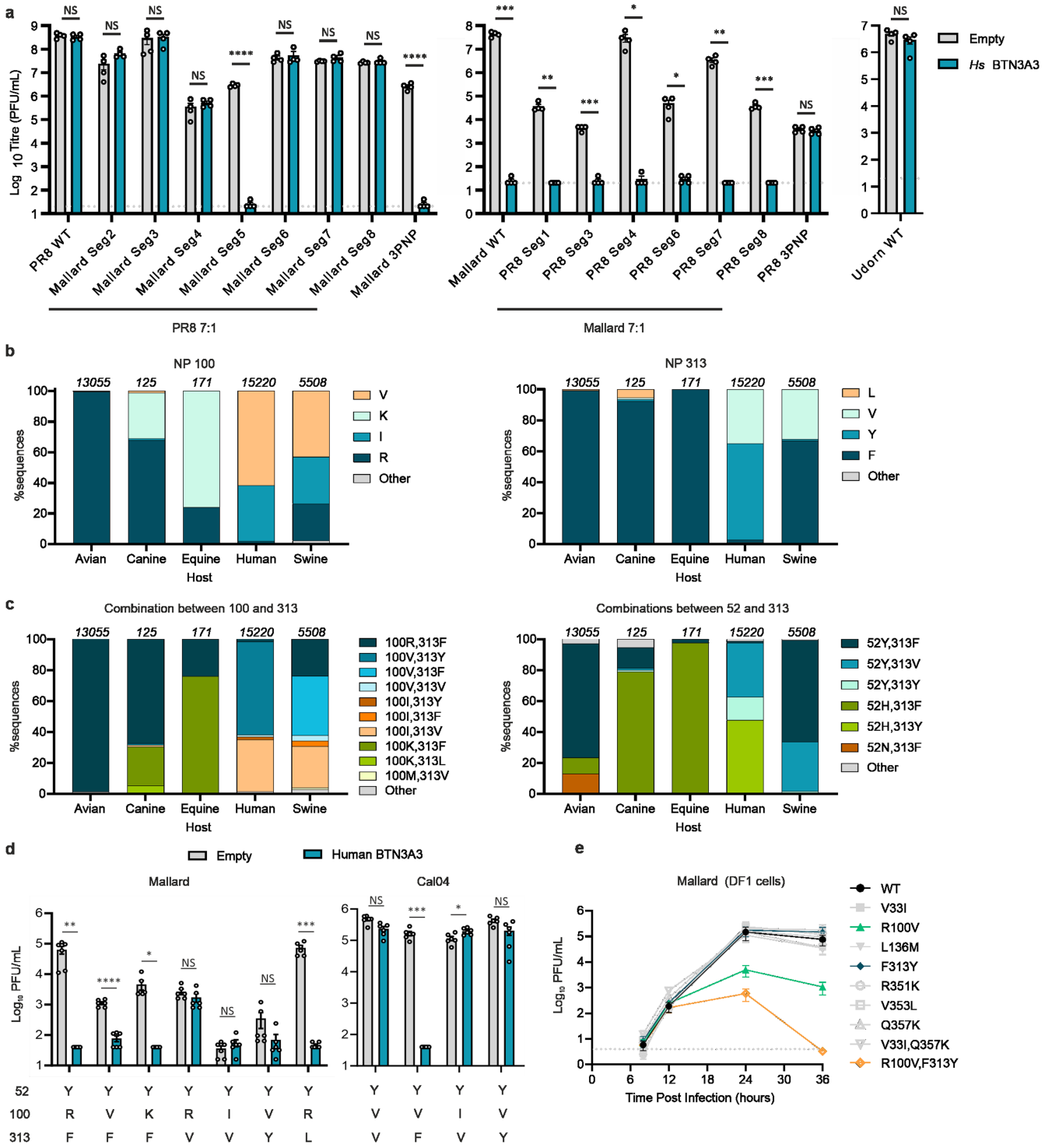

Extended Data Fig. 5 | Determinants of BTN3A3 sensitivity. a, PR8:Mallard reassortants and Udorn wild type (WT) were used to perform plaque assays in MDCK cells expressing BTN3A3 and empty vector control cells. Note that reassortant PR8 7:1 Mallard seg 1, Mallard 7:1 PR8 seg 2 and Mallard 7:1 PR8 seg 5 failed to rescue. Reassortant PR8 Mallard 3PNP is formed by PR8 (segments 4, 6, 7 and 8) and segments 1, 2, 3 and 5 from Mallard. Conversely, reassortant Mallard PR8 3PNP contain segments 4, 6, 7 and 8 from Mallard and segments 1, 2, 3 and 5 from PR8. Data are mean +/− SEM of 2 technical replicates from 2 independent experiments. Statistical differences between cells expressing BTN3A3 and control cells were calculated using multiple t-tests and corrected for multiple comparisons using the Holm-Šídák method. NS-Non-significant, *p ≤ 0.05, **p ≤ 0.01, ***p ≤ 0.001, ****p ≤ 0.0001. **b**, Identity of amino acid residues in positions 100 (left) and 313 (right) of all NP proteins available in our dataset collected from GenBank. **c**, Identity of combinations between amino acid residues 100 and 313 (left) and 52 and 313 (right). **d**, Infectious virus titres obtained in A549-Empty and A549-BTN3A3 cells infected with either Mallard or Cal04 residues 100 and 313 mutants. Cells were infected with an MOI of 0.001 for 48h and viruses were titrated by plaque assay. Data are mean +/− SEM of 2 technical replicates from 3 independent experiments. Statistical analysis was carried out as in (a). **e**, Viral replication assays in avian cells were carried out in chicken fibroblasts (DF1 cells). Cells were infected an MOI of 0.001 for 48 h. Infectious virus titres were determined by plaque assay. Data are mean +/− standard error of the mean (SEM) of 3 independent experiments (each using two technical replicates).

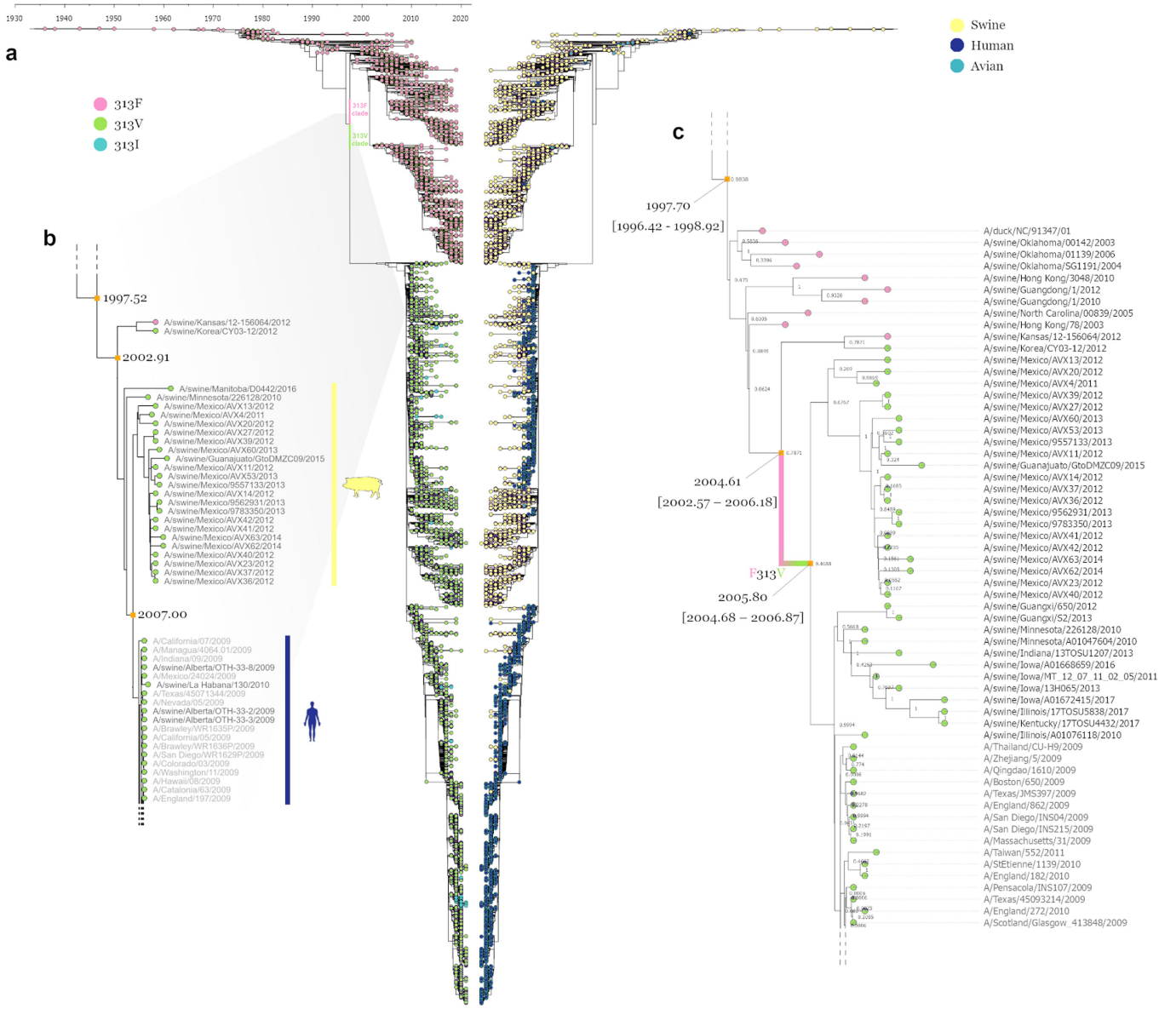

Extended Data Fig. 6 | Molecular dating of the F313V NP substitution on the classical swine H1N1 lineage. a, Tip-dated maximum likelihood phylogeny of all classical H1N1 lineage NP sequences annotated by position 313 residue (left) and isolation host (mirrored tree, right). **b**, Zoomed in snippet of the part of the ML phylogeny shown in A where the F313V change has occurred. Tip shapes are coloured by 313 residue, estimated dates for key nodes are annotated, and strain names are shown on the right of the tips. **c**, Zoomed in snippet of the part of the BEAST maximum clade credibility phylogeny where the F313V change has occurred. Tip shapes are coloured by 313 residue, median node age and 95% highest posterior density confidence intervals are annotated for key nodes, posterior probability values are shown for each node, and strain names are shown on the right of the tips. The branch where F313V is believed to have taken place on is annotated in colour (pink and green). Phylogenies were visualised using FigTree.

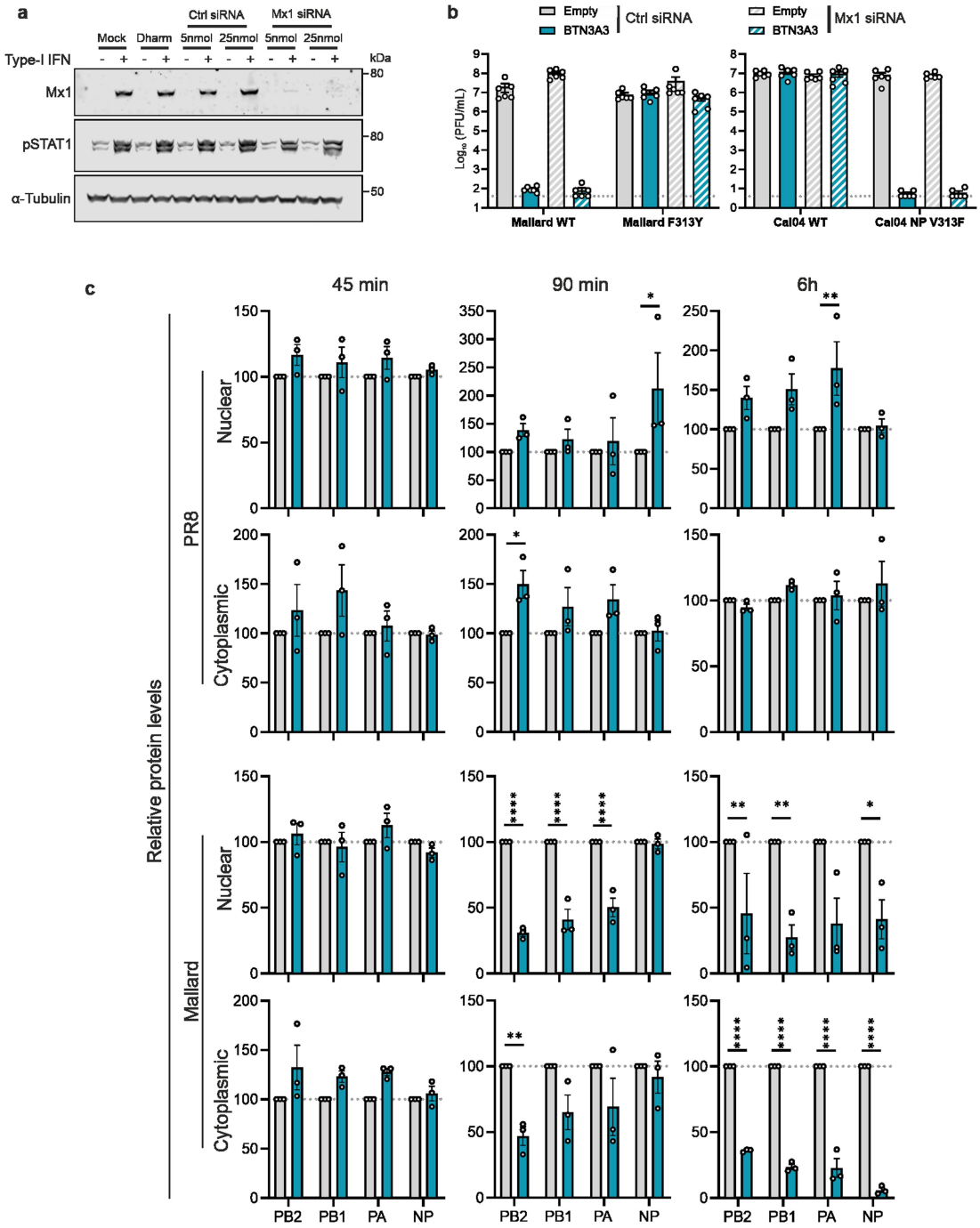

Extended Data Fig. 7 | BTN3A3 activity and its relation to Mx1 and vRNP complexes. a, Western blotting of cell lysates obtained from A549 cells transfected with the indicated amounts of control or Mx1-targeting pooled siRNAs. Cells were transfected for 48h followed by a 16h type-I IFN treatment. pSTAT1 and α-Tubulin were used as IFN-treatment and loading controls, respectively. For gel source data, see Supplementary Fig. 1. **b**, Upon siRNA treatment, A549 Empty and BTN3A3 cells were infected with the indicated viruses at an MOI of 0.001. Supernatants were harvested at 48 hpi and infectious viral titres were measured by plaque assay. Data are mean +/− SEM of 2 technical replicates from 3 independent experiments. **c**, Quantification of cytoplasmic and nuclear levels of vRNP complex proteins at early stages post infection in the presence or absence of BTN3A3. Quantification of 3 independent western blots, one set of which is shown in Fig. 4a. A549-Empty and BTN3A3 overexpressing cells were synchronously infected with PR8 or Mallard at MOI 3. Nuclear/cytoplasm fractionation was performed at 45, 90 mins and 6h post infection. Quantification of vRNP-complex proteins was performed by fluorescence measurements. Cytoplasmic and nuclear viral proteins were normalized to GAPDH and H3, respectively. All values were further normalised to values of A549-Empty cells. Data are mean +/− SEM of 3 independent experiments (each using 2 technical replicates). Statistical significance between groups was measured by a 2-way ANOVA. Comparisons were made between A549-Empty and A549-BTN3A3. NS = non-significant, *p ≤ 0.05, **p ≤ 0.01, ***p ≤ 0.001, ****p ≤ 0.0001.

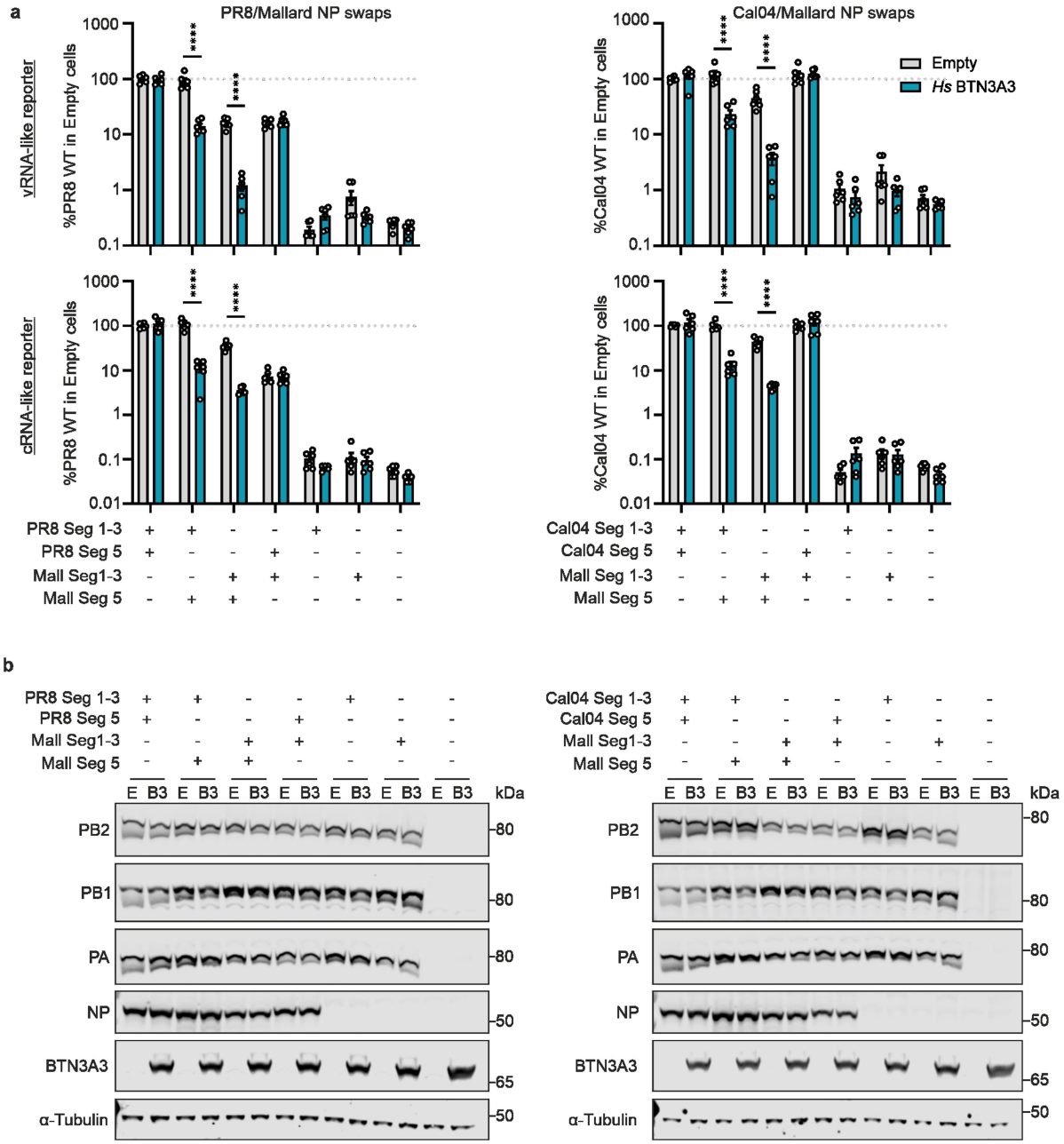

Extended Data Fig. 8 | Minireplicon assays with avian/mammalian NP reassortant RNP complexes. a, 293T-Empty and 293T-BTN3A3 cells were transfected with pcDNA plasmids encoding for PB2, PB1, PA and NP of the indicated viruses alongside firefly luciferase-coding vRNA- or cRNA-like reporter plasmids. A transfection control plasmid expressing *Renilla* firefly was also added. Forty-eight hours post-transection cells were lysed and firefly and *Renilla* luciferase activities were measured. Values were normalised to PR8 or Cal04 WT replicons with respective NPs transfected in 293T-Empty cells. Data are mean +/− SEM of 3 independent experiments (each using 2 technical replicates). Statistical differences between Empty and *Hs*BTN3A3 overexpressing cells were calculated using multiple t-tests and corrected for multiple comparisons using the Holm-Šídák method. NS = non-significant, *p ≤ 0.05, **p ≤ 0.01, ***p ≤ 0.001, ****p ≤ 0.0001. **b**. Expression levels of PB2, PB1, PA and NP transfected in 293T-Empty (E) or 293T-BTN3A3 (B3) cells were assessed by western blot. α-Tubulin was used as loading control. For gel source data, see Supplementary Fig. 1.

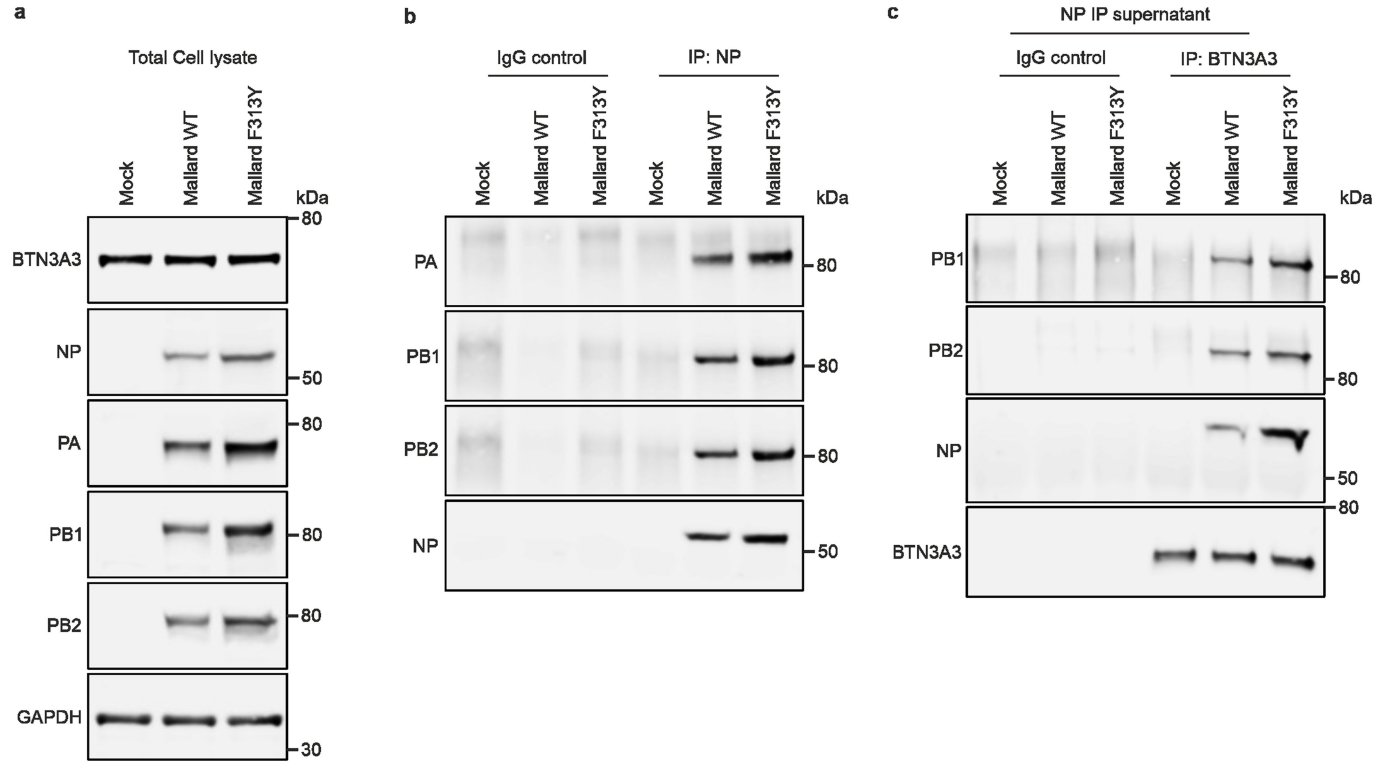

Extended Data Fig. 9 | Interactions between NP and BTN3A3. a, Western blotting of hBEC3-KT cells infected with IAV Mallard WT or Mallard NP F313Y for 6 h. Expression of NP, PA, PB1, PB2 and GAPDH (loading control) from total cell lysates is shown. **b**, Total cell lysates of infected cells were used to perform NP immunoprecipitation followed by the detection of the remaining RNP complex-forming proteins. **c**, Supernatants of the NP immunoprecipitates was used to perform an additional immunoprecipitation using an anti-BTN3A3 antibody followed by the detection of PB2, PB1 and NP. For gel source data, see Supplementary Fig. 1.

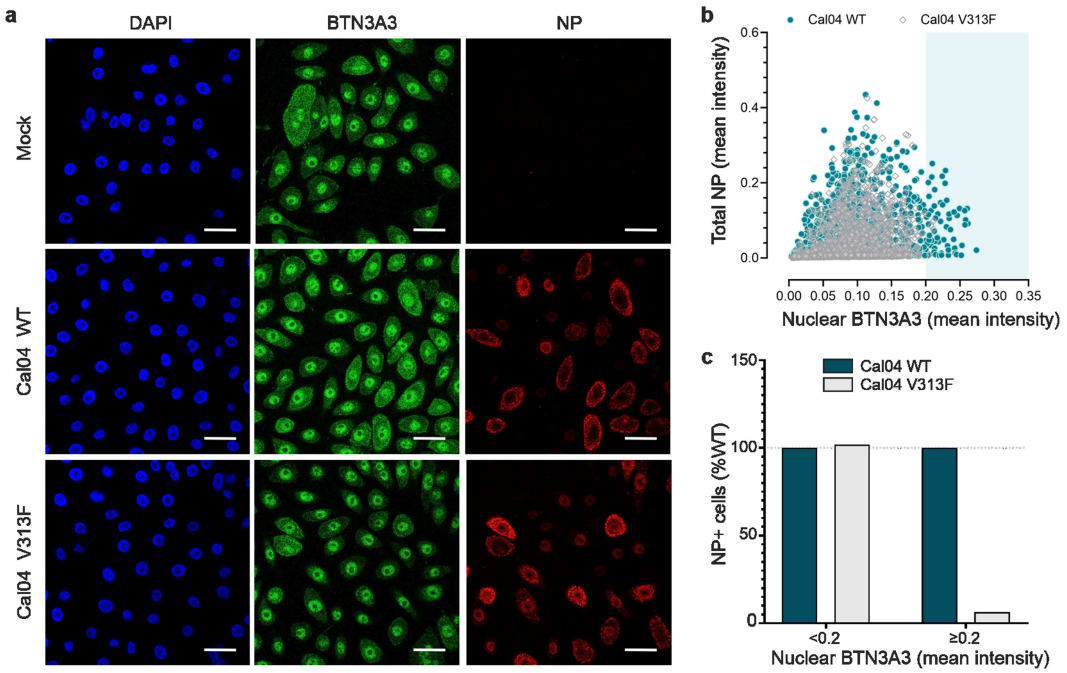

Extended Data Fig. 10 | Correlation between NP signal and nuclear BTN3A3. **a**, Representative images of confocal microscopy of hBEC3-KT cells infected with Cal04WT or Cal04 NP V313F at MOI 3. Six hours post infection, cells were immunostained with NP (red) and BTN3A3 (green). DAPI staining (blue) was used as a nuclear marker. Scale bar = 35µm. **b**, Images from >3500 cells from four independent experiments performed as in (**a**) were used to quantify total NP and nuclear BTN3A3 for Cal04 WT and Cal04 NP V313F. **c**, Values from b were stratified based on nuclear BTN3A3 intensity (<0.2 or ≥0.2). Data represents relative abundance of total infected cells present in each of the two nuclear BTN3A3 intensities ranges, taking values obtained with Cal04 WT as 100%.

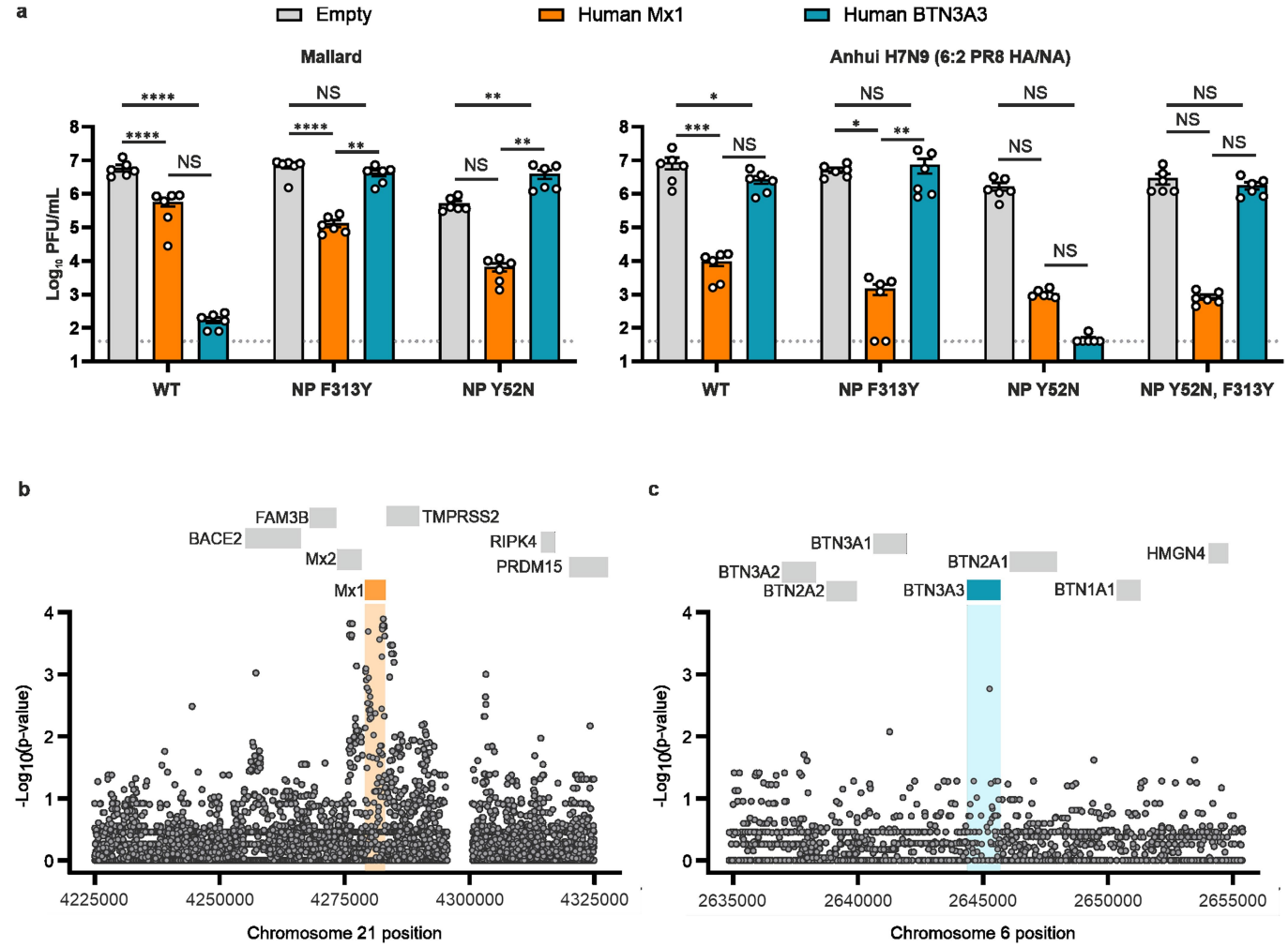

Extended Data Fig. 11 | Distinct requirements of NP residues for BTN3A3 and Mx1 evasion, and GWAS analysis of H7N9 patients. a, A549 cells overexpressing human Mx1 or BTN3A3 were infected with the mentioned viruses at a MOI of 0.001. Supernatants were harvested at 48 hpi and infectious viral titres were measured by plaque assay. Data are mean +/− SEM of 3 independent experiments (each using 2 technical replicates). Statistical significance between groups was measured by a 2-way ANOVA. NS- non-significant, * $p \le 0.05$, ** $p \le 0.01$, *** $p \le 0.001$, **** $p \le 0.0001$. (**b-c**) GWAS analysis of H7N9-infected patients. Manhattan plots of MX1 (**b**) and BTN3A3 (**c**) genomic regions. Gene-level p-values were acquired using RACER in R from data obtained from Chen, et al., *Science* **373**, 918-922, doi:10.1126/science.abg5953 (2021).

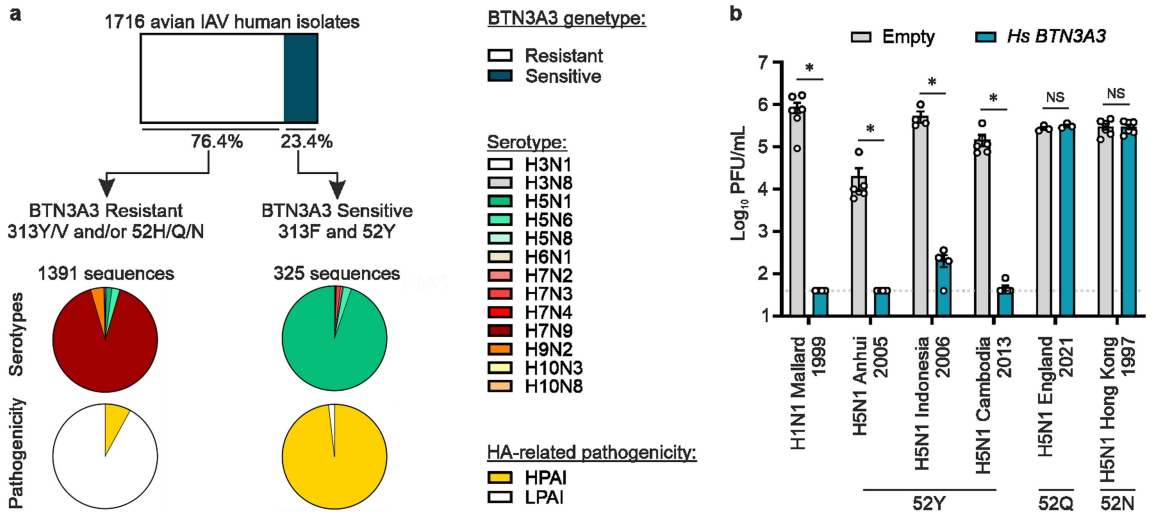

Extended Data Fig. 12 | BTN3A3 restriction by highly pathogenic H5N1. **a**, Schematic representation of numbers and characteristics of avian IAV NP sequences identified in human spillover events. Total number of sequences was divided into BTN3A3-resistant or sensitive genotypes based on amino acid residues 313 and 52. NP sequences were matched with their respective HA sequences and highly pathogenic avian influenza (HPAI) viruses were separated from the low pathogenic (LPAI) based on the presence of a polybasic cleavage site (only present in HPAI isolates). **b**, Replication of 7:1 reassortants of PR8 encoding segment 5 from Mallard or H5N1 HPAI viruses in A549-Empty or A549-BTN3A3 expressing cells. Cells were infected at an MOI of 0.001 for 48h and titres were measured by plaque assay. Data are mean +/− SEM of 3 independent experiments (each using 2 technical replicates) with the exception of 52Q which was instead a single technical replicate from 3 independent experiments. Statistical differences between values obtained in empty and BTN3A3 expressing cells were calculated using multiple t-tests and corrected for multiple comparisons using the Holm-Šídák method. NS = non-significant, *$p \le 0.05$, **$p \le 0.01$, ***$p \le 0.001$, ****$p \le 0.0001$.

nature portfolio

Corresponding author(s): Massimo Palmarini

Last updated by author(s): May 5, 2023

Reporting Summary

Nature Portfolio wishes to improve the reproducibility of the work that we publish. This form provides structure for consistency and transparency in reporting. For further information on Nature Portfolio policies, see our Editorial Policies and the Editorial Policy Checklist.

Statistics

For all statistical analyses, confirm that the following items are present in the figure legend, table legend, main text, or Methods section.

n/a	Confirmed	
☐	☒	The exact sample size (*n*) for each experimental group/condition, given as a discrete number and unit of measurement
☐	☒	A statement on whether measurements were taken from distinct samples or whether the same sample was measured repeatedly
☐	☒	The statistical test(s) used AND whether they are one- or two-sided *Only common tests should be described solely by name; describe more complex techniques in the Methods section.*
☒	☐	A description of all covariates tested
☐	☒	A description of any assumptions or corrections, such as tests of normality and adjustment for multiple comparisons
☐	☒	A full description of the statistical parameters including central tendency (e.g. means) or other basic estimates (e.g. regression coefficient) AND variation (e.g. standard deviation) or associated estimates of uncertainty (e.g. confidence intervals)
☐	☒	For null hypothesis testing, the test statistic (e.g. *F*, *t*, *r*) with confidence intervals, effect sizes, degrees of freedom and *P* value noted *Give P values as exact values whenever suitable.*
☐	☒	For Bayesian analysis, information on the choice of priors and Markov chain Monte Carlo settings
☒	☐	For hierarchical and complex designs, identification of the appropriate level for tests and full reporting of outcomes
☒	☐	Estimates of effect sizes (e.g. Cohen's *d*, Pearson's *r*), indicating how they were calculated

Our web collection on statistics for biologists contains articles on many of the points above.

Software and code

Policy information about availability of computer code

Data collection	Sequences of BTN paralogues/homologues were sourced from NCBI and/or ensemble. IDs are provided in Supplementary Table 5. NP coding sequences unique on the nucleotide level (identical sequences collapsed) were retrieved from the NCBI Flu database (https://www.ncbi.nlm.nih.gov/genomes/FLU/Database/nph-select.cgi?go=database, as of the 8th of June 2021, sampled until the end of 2020). Moreover, during the revision, influeza A segment 5 sequences were also retrieved from GISAID EpiFlu (Supplementary Table s2-4). Acknowledgments for each avian IAV human and bird isolates used in this study are stated in Supplementary Tables 7-8.
Data analysis	Data visualisation and statistical analysis: GraphPad Prism 8 Immunofluorescence imaging acquisition: Zen Microscopy Software (Zeiss) Cytoplasmic/nuclear fluorescent intensity quantification: Cell Profiler Sequence homology search: Blast v.2.8.1 HMM profile protein domain search: HMMER v.3.3 Sequence alignment: Mafft v.7.453 Maximum likelihood phylogenetic inference: iqtree v.1.6.12 Sequence alignment manipulation: pal2nal v.14 Sequence clustering: MMseqs2 v.13.45111 Phylogeny time calibration: TreeTime v.0.9.0 Coding languages: Python v.3.8.5, R v.4.1.3 Phylogeny summary and manipulation: ete3 v.3.1.2 Sequence data summary and manipulation: biopython v.1.76 Tabular information summary and manipulation: pandas v.1.2.4

Phylogeny visualisation: ggtree v.3.2.1, FigTree v.1.4
Bayesian phylogenetic inference: BEAST v.1.10.4, BEAUti v.1.10.4, LogCombiner v.1.10.4

For manuscripts utilizing custom algorithms or software that are central to the research but not yet described in published literature, software must be made available to editors and reviewers. We strongly encourage code deposition in a community repository (e.g. GitHub). See the Nature Portfolio guidelines for submitting code & software for further information.

Data

Policy information about availability of data

All manuscripts must include a data availability statement. This statement should provide the following information, where applicable:

- Accession codes, unique identifiers, or web links for publicly available datasets
- A description of any restrictions on data availability
- For clinical datasets or third party data, please ensure that the statement adheres to our policy

Alignments and raw phylogenetic data related to this study can be found in the following GitHub repository: https://github.com/spyros-lytras/BTN3A3_IAV. Source data related to the animal experiments illustrated in Fig. 3h are available in Enlighten Research Data at the following link: http://dx.doi.org/10.5525/gla.researchdata.1425. Gel source data are available in Supplementary Figure 1.

Human research participants

Policy information about studies involving human research participants and Sex and Gender in Research.

Reporting on sex and gender	*Use the terms sex (biological attribute) and gender (shaped by social and cultural circumstances) carefully in order to avoid confusing both terms. Indicate if findings apply to only one sex or gender; describe whether sex and gender were considered in study design whether sex and/or gender was determined based on self-reporting or assigned and methods used. Provide in the source data disaggregated sex and gender data where this information has been collected, and consent has been obtained for sharing of individual-level data; provide overall numbers in this Reporting Summary. Please state if this information has not been collected. Report sex- and gender-based analyses where performed, justify reasons for lack of sex- and gender-based analysis.*
Population characteristics	*Describe the covariate-relevant population characteristics of the human research participants (e.g. age, genotypic information, past and current diagnosis and treatment categories). If you filled out the behavioural & social sciences study design questions and have nothing to add here, write "See above."*
Recruitment	*Describe how participants were recruited. Outline any potential self-selection bias or other biases that may be present and how these are likely to impact results.*
Ethics oversight	*Identify the organization(s) that approved the study protocol.*

Note that full information on the approval of the study protocol must also be provided in the manuscript.

Field-specific reporting

Please select the one below that is the best fit for your research. If you are not sure, read the appropriate sections before making your selection.

☒ Life sciences ☐ Behavioural & social sciences ☐ Ecological, evolutionary & environmental sciences

For a reference copy of the document with all sections, see nature.com/documents/nr-reporting-summary-flat.pdf

Life sciences study design

All studies must disclose on these points even when the disclosure is negative.

Sample size	For experiments involving quantification of BTN3A3 and NP from immunofluorescence samples, more than 3500 cells were analysed from 4 independent experiments (Figure 5d-f and Extended data figure 13). For the animal experiments, group sizes were chosen on the bases of a pilot experiment to assess AAV transduction and previous experience.
Data exclusions	Lung titres from mice which intranasal infection was not successful were discarded from the analysis (Figure 4g). No other data was excluded.
Replication	For experiments involving quantification of BTN3A3 and NP from immunofluorescence samples, biological variability was observed between experiments. All data from the 4 independent experiments was combined and presented. All replication attempts for the remaining experiments were successful and presented in the respective figures.
Randomization	Fields of infected of mock-infected cells were selected randomly for imaging purposes. For the animal experiments No specific randomisation were conducted. Analysis of data was conducted in an unbiased manner but no specific blinding was used for the researchers carrying out virus titration from mice tissues.

Blinding	Blinding was not performed.

Reporting for specific materials, systems and methods

We require information from authors about some types of materials, experimental systems and methods used in many studies. Here, indicate whether each material, system or method listed is relevant to your study. If you are not sure if a list item applies to your research, read the appropriate section before selecting a response.

Materials & experimental systems

n/a	Involved in the study
☐	☒ Antibodies
☐	☒ Eukaryotic cell lines
☒	☐ Palaeontology and archaeology
☐	☒ Animals and other organisms
☒	☐ Clinical data
☒	☐ Dual use research of concern

Methods

n/a	Involved in the study
☒	☐ ChIP-seq
☐	☒ Flow cytometry
☒	☐ MRI-based neuroimaging

Antibodies

Antibodies used

Primary antibodies:
Rabbit anti-NP polyclonal - Novus Biologicals (NBP2-16965) - used for immunoprecipitation (IP - 3µg/mg of protein lysate) and western-blot (WB - 1:1000)
Mouse anti-NP monoclonal C43 - AbCam (ab128193) - used for WB (1:1000)
Mouse anti-NP monoclonal AA5H - AbCam (ab20343) - used Immunofluorescence (IF) (1:2000)
Rabbit anti-MBP-NP polyclonal (antiserum 2915) - Custom made - used WB (1:500)
Rabbit anti-BTN3A3 polyclonal - Atlas Antibodies (HPA007904) - used for IP (3µg/mg of protein lysate), IF (1:200) and immunohistochemistry (IHC) (1:250)
Rabbit anti-BTN3A3 polyclonal - Proteintech (15896-1-AP) - used for WB (1:750)
Mouse anti-BTN3A3 monoclonal 1A3B5 - Proteintech (67560-1-Ig) used for WB (1:1000)
Rabbit anti-PA polyclonal - Genetex (GTX118991) - used for WB (1:1000)
Rabbit anti-PB1 polyclonal - Thermo Fisher (PA5-34914) - used for WB (1:1000)
Rabbit anti-PB2 polyclonal - Genetex (GTX125926) - used for WB (1:1000)
Rabbit anti-Histone H3 polyclonal - AbCam (ab1791) - used for WB (1:1000)
Rabbit anti-GAPDH monoclonal 14C10 - Cell Signaling Technology (2118S) used for WB (1:10000)
Mouse anti-alpha-Tubulin monoclonal DM1A - Sigma-Aldrich (T6199) used for WB (1:5000)
Rabbit anti-GFP - Cell Signaling (2555s) used for IHC (1:1500)
Rabbit anti-RSAD2 monoclonal (D5T2X) - Cell Signaling (13996S) used 1:1000

Isotype controls:
Rabbit IgG isotype control - Thermo Fisher (02-6102) - used for IP (3µg/mg of protein lysate)
Rabbit serum - Sigma-Aldrich (R4505) - used for IHC (1:250 or 1:1500)

Secondary antibodies:
Anti-rabbit IgG (H+L) (DyLight™ 800 4X PEG Conjugate) - Cell Signaling Technology (5151S) - used for WB (1:10000)
Anti-mouse IgG (H+L) (DyLight™ 680 Conjugate) - Cell Signaling Technology (5470S) - used for WB (1:10000)
Goat anti-Mouse IgG (H+L) Cross-Adsorbed Secondary Antibody, Alexa Fluor™ 555 - Thermo Fisher (A-21422) - used for IF (1:2000)
Goat anti-Rabbit IgG (H+L) Cross-Adsorbed Secondary Antibody, Alexa Fluor™ 488 - Thermo Fisher (A-11008) - used for IF (1:400)

Validation

NBP2-16965: Validation showed by the manufacturer for several techniques (western blot, immunohistochemistry, immunofluorescence, immunoprecipitation and sandwich ELISA). Validated by comparison of mock-infected and infected cells lysates. Migrates at the expected molecular weight.
ab128193: Validation showed by the manufacturer for several techniques (western blot, ELISA, immunofluorescence and flow cytometry). It's has been cited 29 times.
ab20343: Validation showed by the manufacturer for several techniques (immunofluorescence and immunohistochemistry). It's has been cited 82 times.
Custom made rabbit MBP-NP (2915) primary antibody: Validated by comparison of mock-infected and infected cells lysates. Migrates at the expected molecular weight (Digard et al, 1999 - DOI: 10.1128/JVI.73.3.2222-2231.1999)
HPA007904: Validation showed by the manufacturer for several techniques (immunohistochemistry and western blot). Immunohistochemistry validation was performed by Orthogonal validation of protein expression using IHC by comparison to RNA-seq data of corresponding target in high and low expression tissues.
15896-1-AP: Validation showed by the manufacturer for several techniques (western-blot, immunoprecipitation and immunofluorescence).
67560-1-Ig: Validation showed by the manufacturer for western-blot.
GTX118991: Validation showed by the manufacturer for several techniques (western-blot and immunofluorescence). Validated by comparison of mock-infected and infected cells lysates. Migrates at the expected molecular weight. Cited 40 times.
PA5-34914: Validation showed by the manufacturer for several techniques (western-blot, immunofluorescence and CUT&RUN). Cited 4 times.
GTX125926: Validation showed by the manufacturer for western-blot and immunofluorescence. Cited 49 times.

ab1791: Validation showed by the manufacturer for several techniques (western blot, immunocytochemistry, ChIP and Immunoprecipitation). It's has been cited more than 3000 times.
2118S: Validation showed by the manufacturer for several techniques (western blot, immunohistochemistry, immunofluorescence and flow cytometry). It's has been cited more than 5000 times.
T6199: Validation showed by the manufacturer for western blot and immunofluorescence. It's has been cited more than 2000 times.
2555s: Validation showed by the manufacturer for western blot and immunohistochemistry. It's has been cited more than 200 times.
13996S: Validation showed by the manufacturer for western blot. It's has been cited 14 times.

Eukaryotic cell lines

Policy information about cell lines and Sex and Gender in Research

Cell line source(s)	MT4 (gift from Paul Bieniasz, Rockefeller University); Madin-Darby canine kidney (MDCK) cells (ATCC); human embryonic kidney cells (293T) (ATCC); A549 (ATCC); MDCK cells expressing Sialyltransferase 1 (MDCK-SIAT), kindly gifted by John McCauley, The Francis Crick Institute). hTERT-immortalized primary human foetal lung fibroblasts were generated at the CVR. Normal human bronchial epithelial cells immortalised with CDK4 and hTERT (hBEC3-KT) (UT Southwestern Medical Center).
Authentication	MT4 cells and A549 were authenticated using short tandem repeat (STR) analysis carried out by either the DNA Diagnostics Centre (United Kingdom) or Eurofins (United Kingdom), and analysed using the DSMZ online STR analysis tool.
Mycoplasma contamination	Cells were tested for mycoplasma contamination on a bi-monthly basis (average). All experiments were performed in mycoplasma negative cells.
Commonly misidentified lines (See ICLAC register)	No commonly misidentified cell lines were used.

Animals and other research organisms

Policy information about studies involving animals; ARRIVE guidelines recommended for reporting animal research, and Sex and Gender in Research

Laboratory animals	6 week old female C57BL/6 mice
Wild animals	No wild animals were used in this study.
Reporting on sex	Only female mice were used in the study for practical reasons. Male mice fight with each other when housed in the same cage.
Field-collected samples	No field-collected samples were used in this study
Ethics oversight	Animals were maintained at the University of Glasgow under specific pathogen free conditions in accordance with UK home office regulations (Project License PP1902420) and approved by the University of Glasgow ethics committee.

Note that full information on the approval of the study protocol must also be provided in the manuscript.

Flow Cytometry

Plots

Confirm that:

☒ The axis labels state the marker and fluorochrome used (e.g. CD4-FITC).

☒ The axis scales are clearly visible. Include numbers along axes only for bottom left plot of group (a 'group' is an analysis of identical markers).

☒ All plots are contour plots with outliers or pseudocolor plots.

☐ A numerical value for number of cells or percentage (with statistics) is provided.

Methodology

Sample preparation	Cell lines were infected with the mentioned GFP-tagged viruses, trypsined and fixed in 4% formaldehyde.
Instrument	Millipore GUAVA easyCyte HT
Software	Flow cytometry data acquisition was performed using InCyte 3.3 and analysed using FlowJo (v10.6.1).
Cell population abundance	Physical cell sorting was not performed. Only percentage of RFP- and GFP-positive cells was quantified.
Gating strategy	Provided in Supplementary Figure 2

☒ Tick this box to confirm that a figure exemplifying the gating strategy is provided in the Supplementary Information.